



## Aircraft-measured indirect cloud effects from biomass burning smoke in the Arctic and subarctic

L. M. Zamora<sup>1,2</sup>, R. A. Kahn<sup>1</sup>, M. J. Cubison<sup>3</sup>, G. S. Diskin<sup>4</sup>, J. L. Jimenez<sup>3</sup>, Y. Kondo<sup>5</sup>, G. M. McFarquhar<sup>6</sup>, A. Nenes<sup>7,8,9</sup>, K. L. Thornhill<sup>4</sup>, A. Wisthaler<sup>10,11</sup>, A. Zelenyuk<sup>12</sup>, and L. D. Ziemba<sup>4</sup>

<sup>1</sup>NASA Goddard Space Flight Center, Greenbelt, MD, USA

<sup>2</sup>Oak Ridge Associated Universities, Oak Ridge, TN, USA

<sup>3</sup>CIRES and Dept. of Chemistry and Biochemistry, University of Colorado, Boulder, CO, USA

<sup>4</sup>NASA Langley Research Center, Hampton, VA, USA

<sup>5</sup>National Institute of Polar Research, Tokyo, Japan

<sup>6</sup>University of Illinois at Urbana-Champaign, Urbana, IL, USA

<sup>7</sup>Georgia Institute of Technology, Atlanta, GA, USA

<sup>8</sup>Foundation for Research and Technology – Hellas, Patras, Greece

<sup>9</sup>National Observatory of Athens, Athens, Greece

<sup>10</sup>Department of Chemistry, University of Oslo, Oslo, Norway

<sup>11</sup>Institute for Ion Physics and Applied Physics, University of Innsbruck, Innsbruck, Austria

<sup>12</sup>Pacific Northwest National Laboratory, Richland, WA, USA

Correspondence to: L. M. Zamora (lauren.m.zamora@nasa.gov)

Received: 7 August 2015 – Published in Atmos. Chem. Phys. Discuss.: 26 August 2015

Revised: 16 November 2015 – Accepted: 22 December 2015 – Published: 21 January 2016

**Abstract.** The incidence of wildfires in the Arctic and subarctic is increasing; in boreal North America, for example, the burned area is expected to increase by 200–300 % over the next 50–100 years, which previous studies suggest could have a large effect on cloud microphysics, lifetime, albedo, and precipitation. However, the interactions between smoke particles and clouds remain poorly quantified due to confounding meteorological influences and remote sensing limitations. Here, we use data from several aircraft campaigns in the Arctic and subarctic to explore cloud microphysics in liquid-phase clouds influenced by biomass burning. Median cloud droplet radii in smoky clouds were  $\sim 40$ – $60$  % smaller than in background clouds. Based on the relationship between cloud droplet number ( $N_{\text{liq}}$ ) and various biomass burning tracers ( $\text{BB}_t$ ) across the multi-campaign data set, we calculated the magnitude of subarctic and Arctic smoke aerosol–cloud interactions (ACIs, where  $\text{ACI} = (1/3) \times d\ln(N_{\text{liq}})/d\ln(\text{BB}_t)$ ) to be  $\sim 0.16$  out of a maximum possible value of 0.33 that would be obtained if all aerosols were to nucleate cloud droplets. Interestingly, in a separate subarctic case study with low liquid water content

( $\sim 0.02 \text{ g m}^{-3}$ ) and very high aerosol concentrations (2000–3000  $\text{cm}^{-3}$ ) in the most polluted clouds, the estimated ACI value was only 0.05. In this case, competition for water vapor by the high concentration of cloud condensation nuclei (CCN) strongly limited the formation of droplets and reduced the cloud albedo effect, which highlights the importance of cloud feedbacks across scales. Using our calculated ACI values, we estimate that the smoke-driven cloud albedo effect may decrease local summertime short-wave radiative flux by between 2 and 4  $\text{W m}^{-2}$  or more under some low and homogeneous cloud cover conditions in the subarctic, although the changes should be smaller in high surface albedo regions of the Arctic. We lastly explore evidence suggesting that numerous northern-latitude background Aitken particles can interact with combustion particles, perhaps impacting their properties as cloud condensation and ice nuclei.

## 1 Introduction

The incidence of wildfires in the Arctic and subarctic is increasing dramatically (Flannigan et al., 2009; Moritz et al., 2012; Stocks et al., 1998), and in some areas, such as boreal North America, it is expected to grow by 200–300 % over the next 50–100 years (Balshi et al., 2009). Already, periods of intense wildfires can increase regional aerosol concentrations in the Arctic twofold (Warneke et al., 2010), and the impact of smoke is increasingly being recognized as a strong contributor to Arctic haze (Hegg et al., 2009, 2010; McConnell et al., 2007; Shaw, 1995; Stohl et al., 2006, 2007). Increases in biomass burning aerosols could have a large effect on cloud dynamics (Earle et al., 2011; Jouan et al., 2012; Lance et al., 2011; Lindsey and Fromm, 2008; Rosenfeld et al., 2007; Tietze et al., 2011); in turn, smoke-derived changes to cloud microphysics may result in changes to precipitation and regional heating that are strong enough to affect dwindling regional sea ice (Kay et al., 2008; Kay and Gettelman, 2009; Lubin and Vogelmann, 2006; Vavrus et al., 2010).

However, the interactions between smoke particles and Arctic clouds are poorly quantified, in part due to the confounding effects of meteorology and surface conditions (e.g., Earle et al., 2011; Jackson et al., 2012; Jouan et al., 2012), and in part due to satellite sampling constraints over the Arctic, such as caused by the presence of many low contrast regions, multi-layer clouds (Intrieri et al., 2002), and reduced sunlight. One common way in which aerosol–cloud interactions (ACIs) are quantified is by assessing how a cloud property changes relative to some aerosol tracer or, in this case, biomass burning aerosol tracer ( $BB_t$ ). Following Eq. (1), ACI estimates for a given location can be derived from aircraft measurements of cloud droplet number,  $N_{liq}$ ; they can also be derived from ground-based or remote sensing retrievals of changes in cloud properties such as droplet effective radius ( $r_e$ ) or cloud optical depth ( $\tau$ ) at constant liquid water path (LWP) (Feingold et al., 2001; McComiskey et al., 2009):

$$\begin{aligned} ACI &= \frac{1}{3} \frac{d \ln N_{liq}}{d \ln BB_t} = - \left. \frac{\partial \ln r_e}{\partial \ln BB_t} \right|_{LWP} \\ &= \left. \frac{\partial \ln \tau}{\partial \ln BB_t} \right|_{LWP}. \end{aligned} \quad (1)$$

The ACI term as defined by Eq. (1) was originally described as the “indirect effect” (IE) (Feingold et al., 2001, 2003). Here, similarly to McComiskey et al. (2009), we use “ACI” instead of “IE” to differentiate the fact that the metric in Eq. (1) is more directly associated with aerosol-driven changes to cloud microphysical responses than with radiative forcing.

The maximum value of ACIs as derived from Eq. (1) is 0.33. An ACI value of 0.33 corresponds with the 1.0 maximum possible change in  $\ln N_{liq}$  relative to  $\ln BB_t$ , which would occur if every aerosol were to nucleate a cloud droplet. The first term of Eq. (1) is divided by 3 in order to cor-

respond with the last two terms, which are derived at constant LWP from the following theoretical relationships:  $r_e \propto LWP/\tau$  (Stephens, 1978) and  $\tau \propto N_{liq}^{1/3}$  (Twomey, 1977). Note that although each term in Eq. (1) should equal each other’s term, in practice, measurement-derived biases can cause apparent differences between the terms. This issue will be discussed further in later sections.

One study convincingly demonstrated that smoke reduces cloud droplet effective radius and enhances cloud albedo in Arctic liquid clouds (Tietze et al., 2011). In that study, modeled  $BB_t$  concentrations were combined with remote sensing of cloud properties, enabling the authors to reduce meteorological bias by basing their conclusions on tens of thousands of clouds sampled over a variety of meteorological conditions throughout the Arctic. Smoke ACI values derived from relative changes in cloud  $r_e$  were estimated to be between 0.04 and 0.11 out of a maximum 0.33. (Note however that in that study, clouds were binned by temperature and pressure, rather than by LWP as in Eq. 1 above.)

However, despite being able to conclusively demonstrate a smoke cloud albedo effect, Tietze et al. (2011) noted that they might have underestimated the magnitude of satellite-derived ACI values because of difficulties constraining aerosol concentrations and locations. They cite a study by Costantino and Breón (2010), where it was demonstrated that not co-locating aerosol–cloud layers in the vertical column dramatically lowered ACI estimates from 0.24 to 0.04 over marine stratocumulus clouds influenced by African biomass burning. This bias seems to be apparent in many ACI estimates globally; from a literature search, McComiskey and Feingold (2012) revealed that remote-sensing-derived ACI values worldwide are lower than those derived from in situ, modeling, and/or ground-based studies. They also showed that in addition to errors in the co-location of clouds and aerosols, the comparatively low spatial resolution of remote sensing observations can further enhance the low bias in ACI estimates.

In the Arctic, these biases can be substantial. In a study in northern Finland, ACI estimates derived over the same general time period and location from both ground-based and remote sensing methods were  $\sim 0.25$  and  $0.09 \pm 0.04$ , respectively (Lihavainen et al., 2010), a more than twofold difference. For reference, the range of Arctic remote-sensing-derived ACI estimates for all aerosol sources is  $-0.01$  to  $0.09$  (Lihavainen et al., 2010; Tietze et al., 2011); in situ, ground-based, and model estimates range between 0.05 and 0.3 (Garrett et al., 2004; Lihavainen et al., 2010; Zhao et al., 2012). The degree of bias at other global sites has led McComiskey and Feingold (2012) to assert that the albedo effect can only be assessed accurately from aircraft or ground-based in situ data.

To better understand the impacts that expected increases in smoke will have on the Arctic, it is important to better constrain remote sensing and model estimates of smoke-

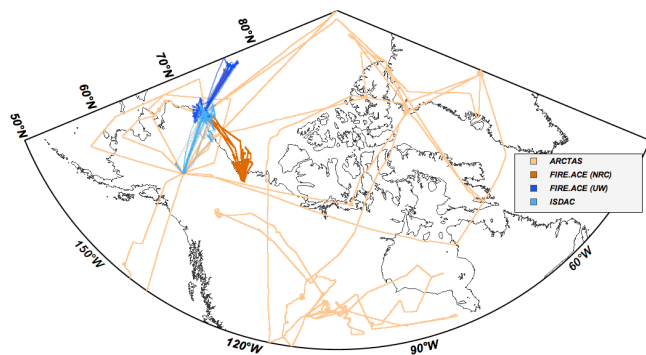


**Figure 1.** Sampling locations for the following campaigns: ARCTAS (light orange), NRC FIRE.ACE (dark orange), UW FIRE.ACE (dark blue), and ISDAC (light blue). The locations of clouds sampled are shown in Fig. 4.

specific ACIs in the Arctic using in situ aircraft data. The biggest challenge in obtaining representative aircraft-based ACI values is the fact that they are more prone to uncertainties caused by the influences of poorly constrained meteorological factors (Shao and Liu, 2006) than other methods due to logistical limitations in sample size. We confront this issue in two ways. First, we focus on a case study day from the Arctic Research of the Composition of the Troposphere from Aircraft and Satellites (ARCTAS) campaign (Fuelberg et al., 2010; Jacob et al., 2010) in which several clouds were sampled under very similar conditions. We derive ACI estimates for all clouds that were either verifiably clean or are clearly influenced by biomass burning aerosols, and contrast the observed cloud properties. Second, to increase sample size, we consolidated data from four separate aircraft campaigns in the Arctic. In addition to ARCTAS, these data sets include: the First ISCCP (International Satellite Cloud Climatology Project) Regional Experiment Arctic Clouds Experiment (FIRE.ACE), which included portions flown by the University of Washington Convair-580 (UW FIRE.ACE) and the Canadian National Research Council Convair-580 (NRC FIRE.ACE) (Curry et al., 2000), and the Indirect and Semi-Direct Aerosol Campaign (ISDAC) (McFarquhar et al., 2011). We then compare these findings with those from the ARCTAS case study.

## 2 Methods

### 2.1 Data set description

The dates and flight locations of data used in this study are shown in Fig. 1, and the data used are listed in Tables 1–4. The ARCTAS, FIRE.ACE, and ISDAC data sets have each been extensively described previously (e.g., Curry et al., 2000; Fuelberg et al., 2010; Jacob et al., 2010; Korolev et al., 2003; McFarquhar et al., 2011; Rangno and Hobbs, 2001; Soja et al., 2008). However, to our knowledge, they

have never been compared directly to each other. Here we note only briefly a few relevant points about the data sets and how they are inter-compared.

First, during the ISDAC and FIRE.ACE flights, multiple passes inside clouds were often obtained, and aerosols were intentionally sampled above- and below-cloud. In contrast, during ARCTAS there was very limited resampling of a given region and generally only one pass through a cloud was obtained. This difference in sampling impacts our results only in that there are not as many vertical profiles through the ARCTAS clouds as in the other data sets. Second, the UW FIRE.ACE data set contains some gaps in positional data (latitude, longitude, and altitude), which range most frequently between 1 and 10 s, with rare instances of gaps > 1 min. If the data were out-of-cloud and if the gap in positional data is < 1 min, we linearly interpolate the latitude, longitude, and/or altitude. Otherwise, occasional gaps > 1 min and data without positional information were excluded. Thirdly and most importantly, we have made our best effort to use data that are as comparable as possible between campaigns. However, when high-quality measurements are not available from the same instrument in all campaigns, we use the most similar measurement available and we discuss the uncertainties this raises in the text.

## 2.2 Cloud presence and phase

### 2.2.1 ARCTAS

In ARCTAS, cloud liquid water content (LWC) was determined from droplet size spectra gathered with the CAPS-CAS instrument (Baumgardner et al., 2001) based on integrated volume droplet size distributions between 0.75 and 50  $\mu\text{m}$ . Throughout this size range, precision was estimated to be 20 % within each size bin based on pre-calibrations with sized glass and polystyrene latex spheres. We expect accuracy to also be  $\sim 20\%$ , since pre-campaign calibrations were performed with spheres of known size, and since post-campaign tests with latex spheres were consistent with the expected sizes. Unfortunately, we could not validate in situ accuracy because simultaneously collected hot-wire probe LWC data were unobtainable due to high noise in out-of-cloud samples. For this reason, in-cloud hot-wire LWC data are not reported here other than to note that they showed qualitatively consistent trends with the CAPS-CAS LWC data. Liquid-phase cloud presence was defined by LWC values  $\geq 0.01 \text{ g m}^{-3}$  (Matsui et al., 2011), a value that corresponds well with cloud presence verified from the on-flight video. Because neither ice water content (IWC) nor cloud particle images were directly measured during ARCTAS, we are unable to accurately verify cloud phase at temperatures  $< 0^\circ\text{C}$  in the ARCTAS data set. Therefore, we limited our focus within the ARCTAS data set to clouds present at temperatures  $> -0.5^\circ\text{C}$  (i.e., those clouds highly likely to be in the liquid phase). We also excluded clouds that the video

**Table 1.** Instrumentation used in this study from the ARCTAS data set. Data were collected at 1 s resolution, unless noted otherwise.

ARCTAS-A 1–19 April; -CARB 29 June; -B 1–13 July 2008			
	Instrument	Range	Uncertainty
$N_{\text{liq}}$ , $r_e$ , and LWC	Cloud, Aerosol and Precipitation Spectrometer – Cloud and Aerosol Spectrometer (CAPS-CAS)	0.5–50 $\mu\text{m}$	20 % <sup>a</sup>
Phase	none (see text)	liquid only	NA
CN	TSI Condensation Particle Counter (CPC) 3010 TSI CPC 3025 TSI Aerodynamic Particle Sizer (APS) 3321 DMT Ultra-High Sensitivity Aerosol Spectrometer (UHSAS)	> 0.01 $\mu\text{m}$ > 0.003 $\mu\text{m}$ 0.583–7.75 $\mu\text{m}$ 0.0609–0.986 $\mu\text{m}$	precision 5 % precision 10 % NA ~ 5 %, but increases in air with > 3000 particles $\text{cm}^{-3}$ (Cai et al., 2008)
Temperature	Rosemount 102 E4AL	–65 to +35 °C	$\pm 1$ °C
Relative humidity	Aircraft-Integrated Meteorological Measurement System (AIMMS-20)	–	2 %
CCN	DMT continuous-flow, stream-wise thermal-gradient CCN counter	–	7–16 % (Moore et al., 2011)
CO	Tunable Diode Laser Absorption Spectrometer (TDLAS)	–	$\pm 2$ % (Sachse et al., 1987)
Submicron sulfate <sup>b</sup>	Time-of-Flight Aerosol Mass Spectrometer	–	$\pm 35$ % (DeCarlo et al., 2008)
Submicron OA <sup>b</sup>	Time-of-Flight Aerosol Mass Spectrometer	–	38 % (Huffman et al., 2005)
BC mass <sup>b</sup>	Single-Particle Soot Photometer (SP2)	–	$\pm 10$ % (Moteki and Kondo, 2008)
CH <sub>3</sub> CN	Proton Transfer Reaction – Mass Spectrometer (PTR-MS)	–	$\pm 10$ % (Wisthaler et al., 2002)
CH <sub>2</sub> Cl <sub>2</sub> <sup>c</sup>	Electron Capture Detection and Mass Spectrometer	–	$\pm 10$ % or $\pm 2$ pptv (Colman et al., 2001)
Total backscatter (550 nm) <sup>b</sup>	TSI 3563 Integrating Nephelometer	> 0.1 $\text{Mm}^{-1}$	0.5 $\text{Mm}^{-1}$
Submicron scatter (550 nm) <sup>b</sup>	Radiance Research Model M903 Nephelometer	1 $\text{Mm}^{-1}$	0.5 $\text{Mm}^{-1}$

<sup>a</sup> Based on pre- and post-campaign comparisons with sized glass and latex spheres. <sup>b</sup> Data were collected at 10 s resolution. <sup>c</sup> Data were collected at ~40 s resolution.

**Table 2.** Instrumentation used in this study from the ISDAC data set. Data were collected at 1 s resolution.

ISDAC, 1–29 April 2008			
	Instrument	Range	Uncertainty
$N_{\text{liq}}$ , $r_e$ , LWC	DMT Cloud Droplet Probe (CDP)	2–50 $\mu\text{m}$	~ 20 % (Earle et al., 2011)
$N_{\text{liq}}^*$ , LWC, $r_e$	Forward Scattering Spectrometer Probe (FSSP) model 100	0.3–47 $\mu\text{m}$	~ 17 % ( $N_{\text{liq}}$ ), ~ 34 % (LWC, $r_e$ ) (Baumgardner, 1983)
Phase	Cloud Particle Imager (CPI)	40 $\mu\text{m}$ –2 mm	NA
CN	PMS airborne Passive Cavity Aerosol Spectrometer Probe (PCASP)-100X TSI CPC 3775	~ 0.12–3 $\mu\text{m}$ > 0.004 $\mu\text{m}$ (Shantz et al., 2014)	7 % (Earle et al., 2011) $\pm 10$ % (Shantz et al., 2014)
Temperature	Rosemont 102 probe	–65 to +35 °C	$\pm 1$ °C
CCN	DMT continuous-flow, stream-wise thermal-gradient CCN counter (reported between 14 and 37 % supersaturation)	–	7–16 % (Moore et al., 2011)
Total and submicron dry backscatter (550 nm)	TSI 3563 Integrating Nephelometer	> 0.1 $\text{Mm}^{-1}$	1–2 $\pm$ 0.5 $\text{Mm}^{-1}$

\* For days when high-quality CDP data were unavailable, following Earle et al. (2011).

**Table 3.** Instrumentation used in this study from the NRC FIRE.ACE data set. Data were collected at 1 s resolution.

NRC FIRE.ACE, 1–29 April 1998			
	Instrument	Range	Uncertainty
$N_{\text{liq}}$	FSSP-100	0.3–47 $\mu\text{m}$	$\sim 17\%$ (Baumgardner, 1983)
LWC, $r_e$	FSSP-100	0.3–47	up to 25 % (Peng et al., 2002)
LWC	King probe	0.05–3 $\text{g m}^{-3}$	$\pm 10\%$ or larger (Peng et al., 2002)
	Nevzorov probe	$\sim 0.006\text{--}1 \text{ g m}^{-3}$	$\pm 15\%$ (Korolev et al., 1998)
Phase	CPI	40 $\mu\text{m}$ –2 mm	not available
Temperature	Rosemont probe	–65 to +35 $^{\circ}\text{C}$	$\pm 1^{\circ}\text{C}$ in-cloud, $\pm 2\text{--}3^{\circ}\text{C}$ out-of-cloud
CN	PCASP 100X	0.12–3 $\mu\text{m}$	7 % (Earle et al., 2011)
CCN	Cloud condensation nucleus counter (reported at 57–72 % supersaturation)	NA	$\pm 10\%$

**Table 4.** Instrumentation used in this study from the UW FIRE.ACE data set. Data were collected at 1 s resolution.

UW FIRE.ACE, 19 May–24 June 1998			
	Instrument	Range	Uncertainty
$N_{\text{liq}}$	FSSP-100	0.3–47 $\mu\text{m}$	$\sim 17\%$ (Baumgardner, 1983)
LWC, $r_e$	FSSP-100	0.3–47 $\mu\text{m}$	see Table 5
LWC	Gerber Scientific PVM-100X	0.01–0.75 $\text{g m}^{-3}$	12 % (Garrett and Hobbs, 1999)
Phase	CPI	40 $\mu\text{m}$ –2 mm	NA
CN	PCASP 100X	0.12–3 $\mu\text{m}$	7 % (Earle et al., 2011)
Total dry backscatter (550 nm)	MS Electron Integrating Nephelometer	$> 0.1 \text{ M m}^{-1}$	NA

indicated were affected by drizzle or ice precipitation from cloud layers above.

## 2.2.2 FIRE.ACE and ISDAC

During the UW and NRC FIRE.ACE campaigns, LWC was determined from droplet size spectra gathered from the Forward Scattering Spectrometer Probe (FSSP-100) measurements for particles with diameters between 0.5 and 47 and 5 and 47  $\mu\text{m}$ , respectively. These measurements are functionally very similar to the CAPS CAS measurements from ARCTAS. During the sampling periods where air mass classification matched the criteria described in Sect. 2.4, the FSSP data had a close relationship to hot-wire probe measurements of LWC for both campaigns (Table 5). For the NRC FIRE.ACE campaign, two FSSP probes were available (serial numbers 96 and 124, denoted hereafter as FSSP-96 and FSSP-124). The FSSP-96 is normally recommended for use by the data originators because the FSSP-124 had an intermittent hardware problem during the NRC FIRE.ACE campaign, and because it may have undersized particles  $> 30 \mu\text{m}$  diameter. In this analysis, the hardware problem did not occur during our time periods of interest, and the FSSP-124 droplet distribution for droplets with diameters within 30–47  $\mu\text{m}$  closely matched those of the FSSP-96. However, the FSSP-124 had higher droplet numbers in particles with diameters  $< 30 \mu\text{m}$  compared to the FSSP-96 during the rel-

evant sampling periods used in this study. We believe this discrepancy to be due to a deficiency in the FSSP-96 data during this time period, because the FSSP-96 underestimated King and Nevzorov probe LWCs by  $\sim 23$  and 26 %, respectively, whereas the FSSP-124 data estimated King and Nevzorov probe data to within 8 %, on average (Table 5). Therefore, the FSSP size distribution data reported here for the NRC FIRE.ACE campaign are based on FSSP-124 data between 5 and 47  $\mu\text{m}$ .

During ISDAC, LWC was determined from cloud droplet probe (CDP) data. These data agreed within 15 % of the bulk probe values. Following Earle et al. (2011), FSSP data were used on days when high-quality CDP data were unavailable; the FSSP data are estimated to agree with CDP data to within 20 %. Note that similarly to ice particles (e.g., Korolev et al., 2011), very large droplets may shatter on any of the cloud droplet probe tips. This may introduce some potential artifacts when droplet sizes are very large (e.g., for some of the reference measurements available in FIRE.ACE and ISDAC).

For comparability with ARCTAS clouds, the presence of liquid clouds in the FIRE.ACE and ISDAC data sets was determined by simultaneous measurements of LWC  $> 0.01 \text{ g m}^{-3}$ . Also, for inter-campaign comparisons we focused on clouds sampled for  $\geq 20$  s in order to both increase representativeness of the average measured properties of the clouds and to enhance meteorological similarity

**Table 5.** Comparison of LWC measurements ( $\text{g m}^{-3}$ ) from various instruments.

Campaign	LWC determination method	Slope	y intercept	$R^2$ value
UW FIRE.ACE	FSSP vs. Gerber Scientific PVM-100X <sup>a</sup> (Gerber et al., 1994)	0.92	−0.018	0.88
NRC FIRE.ACE <sup>b</sup>	FSSP-124 vs. King probe (King et al., 1978)	1.08	−0.006	0.96
	FSSP-124 vs. Nevzorov probe (Korolev et al., 1998)	1.01	0.045	0.82
	Nevzorov vs. King	0.87	0.001	0.82

<sup>a</sup> For Gerber LWC  $< 0.5 \text{ g m}^{-3}$ . Above that, the FSSP missed known rain/drizzle events with larger droplets, and that began to impact the linear relationship. <sup>b</sup>Samples with LWC  $<$  the detection limit were not included.

of clouds. Sometimes entrainment from outside air caused pockets of low to no LWC (i.e., LWC  $< 0.001 \text{ g m}^{-3}$ ) within a cloud body; these pockets of air were not included when determining the average cloud droplet effective radius.

There is no consistent definition for cloud phase in the literature. In remote sensing studies for example, cloud phase is usually determined by cloud radiative properties – thus, clouds with some mixed particles can be included in liquid- or ice-phase classifications if they are mostly liquid or mostly ice (e.g., Baum et al., 2012; Platnick et al., 2003). Due to instrumentation limitations, aircraft studies sometimes also define a cloud with small fractions of ice particles as being a “liquid” cloud (e.g., Korolev et al., 2003). Alternatively, distinct portions of a cloud may be classified as different phases if a primarily liquid portion of a cloud is far away ( $\sim 1\text{--}2 \text{ km}$ ) from a mixed portion of a cloud mass (McFarquhar et al., 2007; Zuidema et al., 2005).

Here, we define liquid cloud phase by the lack of any ice particles in the CPI data throughout the entire cloud transect, based on a roundness criterion (Lawson et al., 2001). When possible (i.e., in the NRC FIRE.ACE and ISDAC data sets), we verified that there was no detectable ice water along the cloud transects. This relatively stringent definition of liquid phase clouds is used to describe as best as possible the liquid-phase end-member cloud characteristics. Because aircraft cloud transects can only sample a portion of a cloud, we must assume that the portion of the cloud sampled is representative of the rest of the cloud. This may introduce uncertainties, particularly in persistent large-scale stratus clouds. Nonetheless, as discussed in Sect. 3.1, we believe that errors from this assumption are not likely to have a large impact on our results.

### 2.3 Cloud microphysical properties

We used aircraft vertical profiles to assess cloud droplet effective radius ( $r_e$ ), cloud liquid water path (LWP) and cloud optical depth ( $\tau$ ), and to gather information on aerosol properties above and below cloud. The  $r_e$  was derived by Eq. (2), following Hansen and Travis (1974):

$$r_e = \frac{\int r^3 n(r) dr}{\int r^2 n(r) dr}, \quad (2)$$

where  $r$  is the radius and  $n(r)$  is the cloud particle size distribution. LWP is defined as the vertical integral of LWC from the base to the top of the cloud. LWP values were only determined when vertical profiles through the cloud were available, thus providing the cloud base and top heights. We define  $\tau$  following Peng et al. (2002) as

$$\tau = \frac{3}{2} \frac{\text{LWC } H_c}{r_e \rho_w}, \quad (3)$$

where  $H_c$  is cloud thickness (again only available in vertical cloud transects) and  $\rho_w$  is the density of water. In addition to vertical transects, we also used horizontal transects within clouds to obtain information on horizontal variability of within-cloud properties and to obtain increased sample numbers for  $r_e$ .

In some instances in the multiple-campaign analysis, the same cloud or very similar clouds were sampled more than once, often intentionally, either through an entire vertical cloud transect or through a portion of a cloud. In order to reduce the potential for pseudo-replication in the analysis, transects that were deemed to be from the same cloud or from very similar clouds were averaged to provide one aggregated profile or  $r_e$  and  $N_{\text{liq}}$  value for those instances. Clouds were determined as being related in part by a combination of time and location sampled. Here, the range of distance and time between clouds deemed as related or the same ranged from 0.4 to 76 km and several seconds to 2.5 h apart, depending on the conditions and cloud type (the 2.5 h time frame included eight separate transects through a stratus cloud). In addition, in all clouds we assessed cloud pressure, location, temperature, and on-flight video (when available). In biomass burning cases we also assessed nearby aerosol conditions (as determined in ISDAC by SPLAT II particle composition and in ARCTAS by  $\text{CH}_3\text{CN}$ , black carbon (BC), submicron  $\text{SO}_4^{2-}$  and submicron organic aerosol, or OA, concentrations). Within the multi-campaign analysis, two of the eight biomass burning clouds contained aggregated transects, as did four of the 16 background clouds. One background

cloud in the case study included aggregated transects. To assess the impact of cloud transect aggregation on our analysis, we calculated differences in ACI values using the maximum and minimum values of  $N_d$  within the aggregated samples. Calculated differences in ACI values were 1 %, indicating that uncertainties caused by aggregation had only minor impacts on our results.

LWC among aggregated clouds was generally similar (within 30 % of each other). However, in some cases it was more variable; in one biomass burning aggregation, the set of eight related cloud transects had LWCs ranging from 0.12 to 0.54 g m<sup>-3</sup>. The relationship of LWC with  $r_e$  suggests that entrainment could have influenced LWC variability within this particular cloud. Although we cannot constrain the influence of entrainment to a high degree of certainty within an individual cloud aggregate, as discussed in Sect. 3.1, the ACI values derived across all clouds did not deviate from adiabatic values calculated from cloud parcel theory.

## 2.4 Air mass classification

For this work, distinguishing smoke-influenced conditions from background cloud conditions is critical. During ARCTAS, background conditions were selected by a combination of in-cloud gas concentrations (average CO < 123 ppbv and average acetonitrile (CH<sub>3</sub>CN) < 0.14 ppbv) and near-cloud SO<sub>4</sub><sup>2-</sup> and BC concentrations (< 0.3 μg m<sup>-3</sup> and < 0.12 μg C m<sup>-3</sup>, respectively). In ideal cases, near-cloud air masses were defined as half the width of the cloud if it was a vertical profile, and within 10 s before and after the cloud if it was a horizontal transect. However, sometimes the presence of a neighboring cloud or the vertical changes in the aircraft track forced us to use slightly smaller samples.

The 123 ppbv CO cutoff value represents the upper quartile range of time periods with concurrently low CO, CH<sub>3</sub>CN, and BC (all separate indicators of combustion), and the CH<sub>3</sub>CN cutoff is the median for these values. For comparison, Latham et al. (2013) and Moore et al. (2011) defined background air masses as having CO and CH<sub>3</sub>CN values at < 170 and 0.1 ppbv, respectively, and Lance et al. (2011) used a criterion of ~ 160 ppbv CO. Such high background CO values are observed periodically over springtime Alaska due to higher emissions from Asia during spring and reduced photochemical loss during winter months (Brock et al., 2011). In 2008 specifically (during a similar time period as ARCTAS-A), background CO was elevated further due to unusually early and frequent Asian wildfires that year (Moore et al., 2011). However, background Arctic CO levels can frequently be lower than these values. For example, during a separate summer campaign in 2011 over eastern Canada, Sakamoto et al. (2015) observed and used a lower background CO threshold of 120 ppbv. Our chosen CO threshold of 123 ppbv was chosen in part because it enabled the use of a consistent value to characterize background con-

ditions across the wide temporal and spatial region covered during ARCTAS.

ARCTAS biomass-burning-influenced air masses were classified following the procedure of Latham et al. (2013), where BB-influenced air masses have concentrations of > 175 ppbv and 0.2 ppbv CO and CH<sub>3</sub>CN, respectively. A manual scan indicated that aerosol pollutant tracers BC and submicron SO<sub>4</sub><sup>2-</sup> were always elevated with respect to background concentrations under these conditions in this data set. For comparison, Lance et al. (2011) used a concentration of > 200 ppbv CO for “polluted” (mostly biomass burning) cases.

During the two FIRE.ACE campaigns, the combination of relevant high-quality and/or high-resolution aircraft chemical data for completely characterizing air mass sources was not collected, and remote sensing products useful for air mass classification were also unavailable. As a result, biomass-burning-derived haze events were indistinguishable from anthropogenic pollution events in the FIRE.ACE data sets. Therefore, we only use FIRE.ACE clouds sampled under unpolluted background conditions for inter-comparison with the other data sets.

Because within-cloud gas concentrations were not available, we used average near-cloud (as defined above) aerosol concentrations to define background conditions in the FIRE.ACE data. To reduce the risk of any potential humidification effects, we excluded near-cloud air masses that had any observations of cloud particles in the CPI or that had LWC values ≥ 0.001 g m<sup>-3</sup>.

To classify background air masses, we used the Passive Cavity Aerosol Spectrometer Probe (PCASP) aerosol concentrations (CN<sub>PCASP</sub>) directly adjacent to the cloud. The PCASP measures dehumidified particles with diameters between 0.12 and 3 μm. Previous authors have noted the presence of large numbers of small nucleation- to Aitken-mode particles (between ~ 15 and 85 nm) in the spring and summertime Arctic that appear to have natural sources (Garrett et al., 2004; Howell et al., 2014; Leaitch et al., 2013; Leck and Bigg, 1999; O’Dowd et al., 2010; Ström et al., 2009; Tunved et al., 2013; Zhao and Garrett, 2015). However, the relatively large minimum size cutoff of the PCASP (~ 120 nm) excludes these particles, while including low altitude particles from pollution and biomass burning sources, which tend to be in the accumulation mode (Earle et al., 2011; Latham et al., 2013; Warneke et al., 2010). Thus, CN<sub>PCASP</sub> tends to be a fairly good indicator of non-background conditions.

To be classified as background, air masses had to have CN<sub>PCASP</sub> concentrations of ≤ 127 particles cm<sup>-3</sup> (Shantz et al., 2012). This CN<sub>PCASP</sub> cutoff is a more stringent criterion for determining clean conditions than those adopted by Jackson et al. (2012), Earle et al. (2011), and Peng et al. (2002), where respective values of < 200, 250, and 300 particles cm<sup>-3</sup> were used, but the criterion applied here appears to exclude biomass burning and pollution aerosols fairly effectively (Table 6). However, the upper 95 % CH<sub>3</sub>CN

**Table 6.** A comparison of background concentrations of biomass burning and pollution tracers as previously reported to those in the ARCTAS-B data set in air masses that would be defined as background using only the  $\text{CN}_{\text{PCASP}}$  equivalent<sup>a</sup> cutoff of  $\leq 127$  particles  $\text{cm}^{-3}$ . Data are out-of-cloud and from altitudes  $< 2.1$  km due to instrument limitations above this level.

Tracer (units)	Median (interquartile range)	95th percentile	Previously reported background <sup>b</sup> concentrations
CO (ppbv)	96 (96–109)	135	120–170 <sup>f,i</sup>
CH <sub>3</sub> CN (ppbv)	0.08 (0.06–0.10)	0.19	0.1 <sup>h,j</sup>
BC ( $\mu\text{g C m}^{-3}$ )	0.001 (0.001–0.004)	0.016	0.029 <sup>f</sup>
Submicron $\text{SO}_4^{2-}$ ( $\mu\text{g m}^{-3}$ ) <sup>c</sup>	0.010 (0.005–0.070)	0.33	0.1–0.9 <sup>f,j-1</sup>

<sup>a</sup>  $\text{CN}_{\text{PCASP}}$  values were not available in ARCTAS, and were thus approximated from the CN concentrations from the APS and UHSAS for the same size range as would be measured in the PCASP. <sup>b</sup> Submicron  $\text{SO}_4^{2-}$  concentrations are reflective of average, not background, conditions. <sup>c</sup> Following Fisher et al. (2011), we assume ARCTAS submicron sea-salt  $\text{SO}_4^{2-}$  is negligible, and that total submicron  $\text{SO}_4^{2-}$  is approximately equal to submicron non-sea-salt  $\text{SO}_4^{2-}$ . <sup>d</sup> Stohl et al. (2007), <sup>e,f</sup> Warneke et al. (2009, 2010), <sup>g</sup> Brock et al. (2011), <sup>h</sup> Moore et al. (2011), <sup>i</sup> Shinozuka et al. (2015), <sup>j</sup> Latham et al. (2013), <sup>k,l</sup> Quinn et al. (2000, 2002).

concentrations are higher than typical background conditions, indicating that our chosen cutoff value is generally, but not completely, effective at removing air masses influenced by smoke. Therefore, the FIRE.ACE samples have a more uncertain background classification than the ARCTAS and ISDAC data sets, where actual chemical tracers verify the presence of pollution and biomass burning aerosols. For ISDAC samples, background conditions were determined by out-of-cloud  $\text{CN}_{\text{PCASP}}$  concentrations, in order to be consistent with the FIRE.ACE campaigns. However, the TSI aerosol concentrations ( $\text{CN}_{\text{TSI}}$ ) and backscatter values were not used to assign a background classification (see Sect. 3.2 for further details).

A biomass burning classification was assigned in ISDAC data when a cloud had contact with discernable amounts of biomass burning aerosols, as determined by single particle mass spectrometer, SPLAT II (Zelenyuk et al. 2009, 2015), based on the mass spectral analysis of individual aerosol particles (Fig. 2). This method has been similarly employed to determine biomass burning influence in the ISDAC data set previously (Earle et al., 2011; McFarquhar et al., 2011; Shantz et al., 2014).

## 2.5 Assessment of indirect effects from biomass burning

As mentioned before, the impact of smoke aerosols on cloud droplet activation was assessed by looking at aerosol–cloud interactions of biomass burning aerosols on cloud droplet number. The ACI values were derived from changes in cloud droplet number relative to measured biomass burning tracers,  $\text{BB}_t$ , following Eq. (1) and using a nonparametric Kendall robust line-fit method. The Kendall robust line-fit model (also commonly known as the Theil–Sen method) (Sen, 1968; Theil, 1950) derives a linear model of a data set from the median of the slopes between each two points in the data set. While this method is not as commonly used as linear regressions, it performs similarly when data are normally dis-

tributed. In cases when the data are not normally distributed, this method is more appropriate than a linear regression because it reduces the impact of outliers.

As previously mentioned, ARCTAS was the only campaign where biomass burning gaseous tracers were directly quantifiable in-cloud (here we use  $\text{BB}_t = \text{CH}_3\text{CN}$  (de Gouw et al., 2003) and  $\text{BB}_t = \text{CO}$  (Tietze et al., 2011)), measured in ppbv. Both CO (Bian et al., 2013) and  $\text{CH}_3\text{CN}$  have appreciable background concentrations in the Arctic (as can be seen in Fig. 3a). Therefore, approximate background CO and  $\text{CH}_3\text{CN}$  concentrations of 99.2 and 0.088 ppbv, respectively, were subtracted prior to deriving ACI values from Eq. (1) in the case study. These background values were derived from the mean of the Kendall robust line-fit method analyses of ARCTAS CCN (cloud condensation nuclei) and  $\text{CN}_{\text{PCASP}}$  equivalent concentrations vs. CO (or  $\text{CH}_3\text{CN}$ ) concentrations. In the multi-campaign analysis, background values of 0.018 ppbv  $\text{CH}_3\text{CN}$  were subtracted, due to lower background concentrations in the cleanest samples. Although for simplicity we define a single background Arctic  $\text{CH}_3\text{CN}$  level here, background  $\text{CH}_3\text{CN}$  can range from  $\sim 0.050$  ppbv in the Arctic marine boundary layer to  $\sim 0.14$  ppbv at altitudes of  $\sim 8$  km (Kupiszewski et al., 2013; Warneke et al., 2009; A. Wisthaler, personal communication, 2015). A maximum error of 0.038 ppbv in background  $\text{CH}_3\text{CN}$  would equal at most 18 % of the  $\text{CH}_3\text{CN}$  signal in biomass burning samples. For that reason, and because  $\text{CH}_3\text{CN}$  was only one of six tracers used to derive ACI values, the range of possible background  $\text{CH}_3\text{CN}$  concentrations is expected to have only minor impacts on the analysis. Arctic background CO is more consistent than  $\text{CH}_3\text{CN}$ , and in that case, the differences in background CO as computed from  $\text{CN}_{\text{PCASP}}$  vs. CCN line-fit analyses (93.0 and 105.4 ppbv, respectively) led to only a 2.6 % change in the derived ACI values.

Because the in-cloud CO and  $\text{CH}_3\text{CN}$  values were not available in the ISDAC or FIRE.ACE campaigns, we also compared aerosol tracers of smoke/polluted particles adjacent to the cloud as a  $\text{BB}_t$  quantity. The aerosol tracers



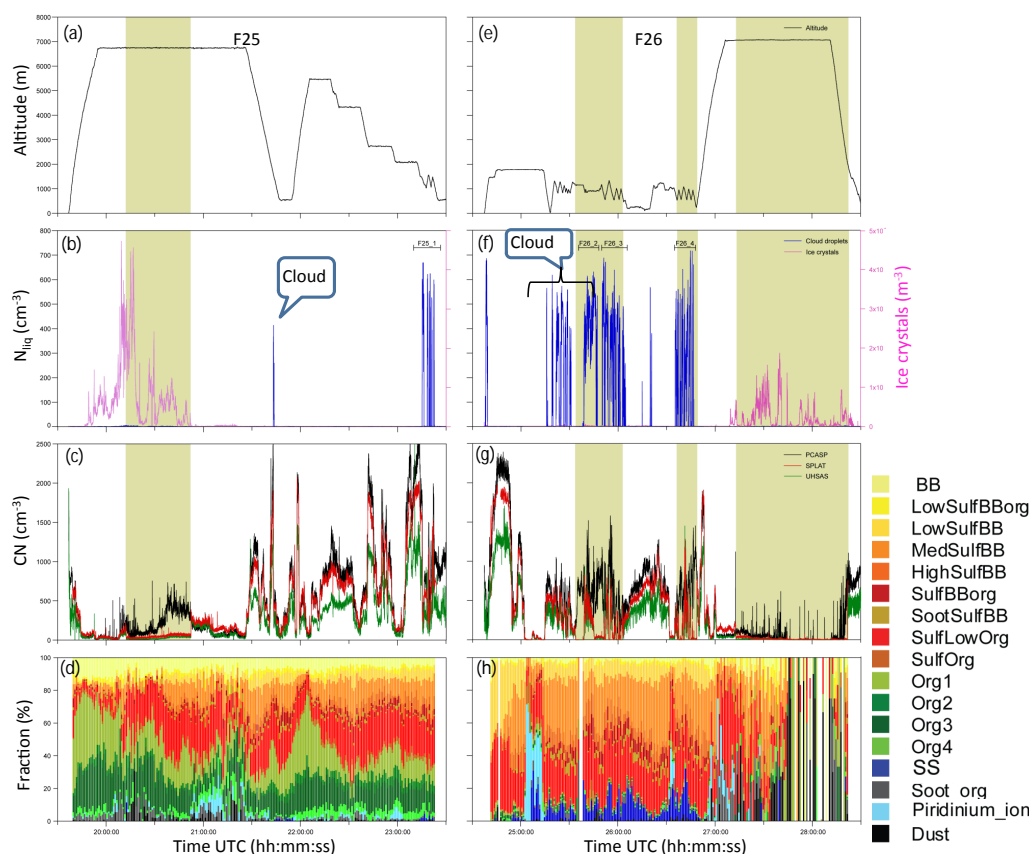


**Figure 2.** ISDAC 2008 aerosol and flight characteristics near and in selected clouds influenced by biomass burning from 19 April (left) and 20 April (right). Flight characteristics shown include: (a) altitude, (b) LWC (blue) and IWC (pink), (c) aerosol concentration from the PCASP (black), SPLAT (red), and UHSAS (green) instruments, and (d) bulk aerosol SPLAT chemical composition. Tan shading indicates SPLAT sampling through the in-cloud CVI inlet.

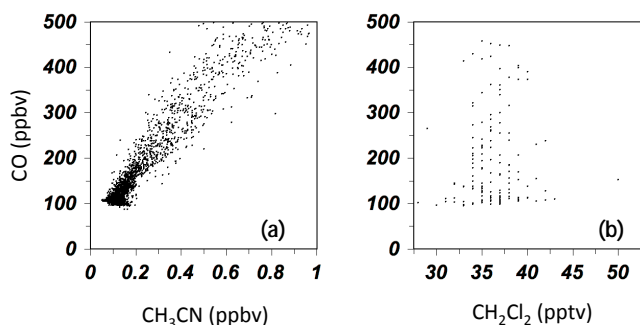


**Figure 3.** Carbon monoxide (ppbv) during the 1 July 2008 ARCTAS-B flight as a function of (a) the biomass burning tracer  $\text{CH}_3\text{CN}$  (ppbv) and (b) the fossil fuel combustion tracer  $\text{CH}_2\text{Cl}_2$  (pptv).

used were  $\text{CN}_{\text{PCASP}}$  concentrations, backscatter at 550 nm, BC concentrations, and when available, CCN (not available in the UW FIRE.ACE campaign). For comparison to the PCASP, aerosol concentrations with diameters  $> 4$  nm were measured with a TSI 3775 in ISDAC. Aerosols with diame-

ters  $> 3$  and  $10$  nm were measured during ARCTAS from TSI models 3025 and 3010, respectively. Because  $\text{CN}_{\text{PCASP}}$  values were not measured during ARCTAS, we combined APS- and UHSAS-sized aerosol data collected during that campaign into a similar size distribution as the  $\text{CN}_{\text{PCASP}}$  measurements ( $0.124\text{--}3.278\ \mu\text{m}$ ). UHSAS and APS measurements are not actively dried like PCASP samples are (Earle et al., 2011; Strapp et al., 1992), but sample humidity decreases significantly upon heating in the cabin and measurements are taken at dry relative humidity; in addition, particles are exposed to dried sheath air prior to detection.

There are some limitations of the ACI approach. First, a systematic bias can be introduced when aerosol and cloud properties are averaged or co-located in low spatial or temporal resolution data sets (McComiskey and Feingold, 2012). This particular systematic bias is generally not a large concern for in-cloud aircraft studies such as this one where gas and/or aerosol measurements and  $N_{\text{liq}}$  measurements are either collected simultaneously or in very close proximity. Secondly, the magnitudes of derived ACIs can vary depending on the  $\text{BB}_t$  tracers used, and any one tracer may be biased by random error and a variety of other reasons that may cause

the tracer to imperfectly approximate actual cloud droplet nuclei. To reduce the biases inherent to any one tracer, we use a combination of up to six  $BB_t$  tracers to derive ACIs, as available.

A third potential problem is the risk that a snapshot of a cloud in time is not representative of the net cloud properties over its lifetime (Duong et al., 2011). Currently, only models can fully characterize cloud lifetime properties, but interpreting the model output can be challenging for other reasons. Within aircraft in situ data, this source of sampling error is best minimized in aircraft in situ data by resampling throughout the cloud's life cycle. Resampling was sometimes, but not always, carried out for individual cloud cases presented here, and was not specifically carried out throughout the lifetime of the cloud. However, based on the results presented in Duong et al. (2011), the magnitude of this type of error is unlikely to have a large impact on our results, although we cannot with full confidence assess how cloud life stage might have impacted the way aerosols were interacting with the clouds.

The fourth limitation of the ACI method is that  $N_{liq}$  has a sublinear relationship with CCN (e.g., Morales et al., 2011; Morales and Nenes, 2010), with particularly noticeable deviations from linear behavior expected when a cloud contains high CCN concentrations (e.g., Moore et al., 2013). This behavior is driven by increased competition for water vapor, which in turn decreases cloud supersaturation and reduces the tendency to form additional drops. Because ACI values are typically derived from linear-type regressions, apparent ACI values can be reduced if clouds with high CCN are included in the analysis. We discuss the potential for this type of interaction where applicable in the text. Finally, the most difficult problem to address is the potential bias introduced if one does not account for meteorological conditions (Shao and Liu, 2006). We discuss the relationship of derived ACIs with meteorology in Sects. 2.6 and 3.

## 2.6 Overview of surface and meteorological conditions

Ambient conditions such as cloud type and presence of drizzle from an overlying cloud deck were determined from available video, photos, flight notes, and AVHRR images. Although in situ chemical and physical measurements were primarily used to determine end-member situations (i.e., where only smoke or only background air were the dominant sources of aerosols interacting with clouds), in some cases we discuss out-of-cloud aerosols with potentially more mixed sources. In these cases we supplemented chemical and physical data with 5-day HYSPLIT back trajectories (Draxler, R. R. and Rolph, G. D. HYSPLIT (HYbrid Single-Particle Lagrangian Integrated Trajectory) model, accessed via the NOAA ARL READY website (<http://www.arl.noaa.gov/HYSPLIT.php>), NOAA Air Resources Laboratory, College Park, MD) to determine recent air mass history. Using video, photos, and flight notes, clouds were also classified as either stratiform or cumuliform. Stratiform clouds were

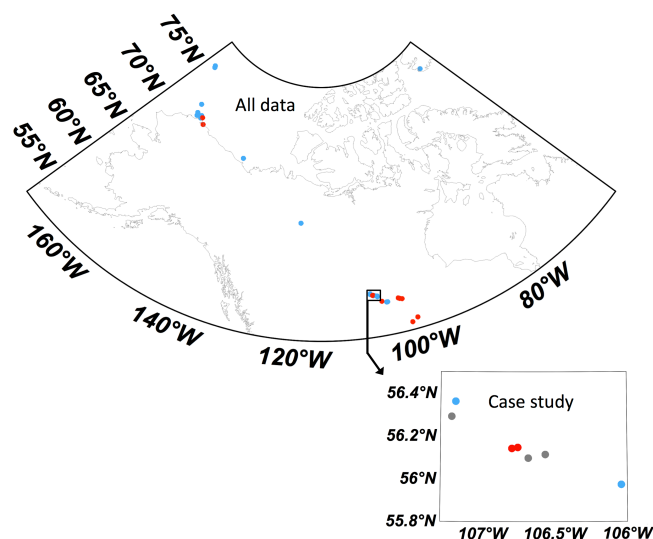


**Figure 4.** Map of cloud sample locations from all campaigns. Red points indicate biomass burning samples, blue cases indicate background samples, and gray points indicate intermediate samples.

present at 1–3 km altitude. With one exception (an ARCTAS-B background case from 8 July 2008), the stratiform clouds were not present below a strong temperature or moisture inversion. In our data set, none of the biomass burning cases were present below an inversion either; such inversions occurred only in four of the clean background cases, indicating generally unimpeded aerosol mixing from above and below for biomass burning clouds in these data. The cumuliform clouds were also found between 1 and 3 km, and although they were less optically thick than the stratiform clouds, optically thin ( $\tau < 15$ ) and multi-layer clouds dominated all samples.

Across all clouds sampled during the four campaigns, there was substantial variation between cloud properties (Table 7) and the physical locations of the clouds (Fig. 4). For example, background clouds were primarily sampled over the open ocean and at higher latitudes, whereas the smoky clouds were primarily sampled at lower latitudes over land. For this reason, in addition to comparing median characteristics of all background and clean cases, we also focus on a case study where multiple clean and smoky clouds were observed under very similar meteorological and surface conditions (Sect. 3.1).

### 3 Results

#### 3.1 Indirect effects of smoke in Arctic liquid-phase clouds

On 1 July 2008 during the ARCTAS-B campaign, a variety of small cumuliform clouds were sampled during flight 18 over inland Saskatchewan, Canada. The physical characteristics of the clouds were very similar (Table 8), being small ( $\sim 0.7$  km high, and  $\sim 0.2$ – $7$  km wide) non-precipitating clouds present between 1680 and 2650 m altitude, and far from any major temperature or water vapor inversions. All clouds were liquid phase, with low median LWC values of  $0.02 \text{ g m}^{-3}$  (the implications of which are discussed further down). All clouds had temperatures ranging from  $-0.1$  to  $3.1$  °C. All were sampled within  $97 \text{ km}^2$  and 5.2 h of each other, during which time each cloud experienced a similar northeasterly wind direction.

Despite being exposed to similar meteorological and surface conditions, aerosol inputs to these clouds ranged significantly, with average  $\text{CH}_3\text{CN}$  and PCASP equivalent particle numbers ranging between 0.092 and 0.55 ppbv and  $107$  and  $3001 \text{ cm}^{-3}$ , respectively. The large range in chemical properties was due to the aircraft track, which repeatedly covered areas up- and downwind of local fresh smoke plumes from the Lake McKay fire. This fire is comprehensively described in the combination of Cubison et al. (2011), Alvarado et al. (2010), and Raatikainen et al. (2012).

In Fig. 3, we show that  $\text{CO} < 500$  ppbv is strongly related to the smoke tracer  $\text{CH}_3\text{CN}$  and that it shows no correlation to the fossil fuel combustion tracer dichloromethane ( $\text{CH}_2\text{Cl}_2$ ) (see Kondo et al., 2011 for further discussion on use of this tracer during ARCTAS). Given that CO has both pollution and biomass burning sources, this finding indicates smoke was the dominant aerosol contributor on that day, not pollution. Back trajectories also support this conclusion (Alvarado et al., 2010). Of the clouds sampled during this flight, two clouds met the classification criteria for being biomass-burning-influenced, three were classified as intermediate, and two met the ARCTAS background criteria.

As shown in Fig. 5, smoke is clearly correlated with reduced cloud droplet radius in the seven clouds studied (with an average 59 % reduction relative to background clouds, Table 8). As expected, there was a concurrent increase in cloud droplet number (Fig. 5). Based on this increase, we compute a combined median ACI of 0.05 (bootstrapped 95 % confidence interval 0.04–0.06) across all tracers shown in Fig. 5.

Although linear regressions were not used to derive ACIs, we plot them for each tracer in Fig. 5 to show the degree of variation between individual tracer ACI values. Other researchers have previously noted differences in calculated ACIs when these interactions are computed from different tracers (e.g., McComiskey et al., 2009; Lihavainen et al., 2010; Zhao et al., 2012), and these differences probably reflect a combination of measurement error and how well

a given tracer approximates the sub-population of aerosols that are participating in cloud droplet activation (Lihavainen et al., 2010). As plumes age, there may also be increasing uncertainty in biomass burning aerosol co-location with gaseous tracers such as CO and  $\text{CH}_3\text{CN}$ , as these are subject to different depositional processes (Hecobian et al., 2011). However, in this case the fires were relatively fresh so this issue is unlikely to be an important source of uncertainty.

ACI estimates can also sometimes be influenced or even overwhelmed by systematic differences in local meteorological conditions associated with cleaner versus more polluted clouds (Hegg et al., 2007; Shao and Liu, 2006). For the case study, that possibility is unlikely because of the relatively small area and time frame considered and the similar meteorological conditions in which the clouds were sampled.

However, because case study smoky clouds had a combination of very low LWC, very high aerosol concentrations from a fresh fire, and consequently, very small droplet sizes (Fig. 6), it is likely that smoky case study clouds were less sensitive to further additions of smoke aerosols than clouds with lower aerosol concentrations. Such nonlinear behavior is predicted when high CCN levels cause increased competition for water vapor, which in turn decreases cloud supersaturation and reduces the tendency to form additional drops (e.g., Moore et al., 2013; Morales et al., 2011; Morales and Nenes, 2010). Additionally, possible enhanced entrainment of outside air in smoky clouds compared to background clouds (Ackerman et al., 2004; Bretherton et al., 2007; Chen et al., 2012; Lebsock et al., 2008) could enhance droplet evaporation and further reduce ACI values from the expected adiabatic ACI maximum value at a given aerosol level.

Because in situ ACI derivations assume linearity in the response of  $N_{\text{liq}}$  to  $\text{BB}_t$ , and such an assumption does not hold well at high CCN levels, we would expect to derive lower in situ ACI estimates if clouds with very high CCN levels are included in the analysis (Rosenfeld et al., 2014). That ACI values would increase to 0.08 (95 % confidence interval 0.05–0.12) if the two biomass burning clouds were excluded suggests that nonlinear processes could have affected the reduced ACI values in the case study. For reference, at case study smoky  $\text{CN}_{\text{PCASP}}$  equivalent concentrations of  $\sim 2000$ – $3000 \text{ cm}^{-3}$ , modeled adiabatic ACI values were  $\sim 0.06$ – $0.16$  (Moore et al., 2013). The range in modeled ACI values depended on factors such as cloud vertical velocity and CCN hygroscopicity (the CCN spectrum). Given these model uncertainties and our estimated case study ACI value, any potential effects of entrainment were not clearly noticeable in our data.

For these reasons, although the 1 July 2008 case is in some ways ideal, in that the clouds were sampled in very similar environmental conditions, it is not necessarily representative of typical cloud conditions in the Arctic. The clouds were present relatively far south in the subarctic ( $52$ – $56^\circ \text{N}$ ) and were cumuliform compared to the more dominant Arctic stratus-type clouds. Moreover, the case study clouds were

**Table 7.** Median properties and ranges for all background and biomass burning cloud cases in the multi-campaign assessment.

Property	Background ( $n = 19$ )	Biomass burning ( $n = 8$ )
Aerosol number concentration ( $\text{CN}_{\text{PCASP}}^*$ ), $\text{cm}^{-3}$	42 (1–97)	584 (58–2001)
CCN, $\text{cm}^{-3}$	31 (6–332)	437 (68–6670)
Backscatter at 550 nm, $\text{Mm}^{-1}$	0.7 (–0.19 to 1.13)	8.8 (0.3–44.1)
Temperature, $^{\circ}\text{C}$	–5 (–20 to 7)	2 (–9 to 10)
Pressure, mbar	848 (505–995)	776 (687–909)
Liquid water content (LWC), $\text{g m}^{-3}$	0.07 (0.01–0.25)	0.03 (0.01–0.27)
Cloud droplet effective radius ( $r_e$ ), $\mu\text{m}$	8.7 (5.7–12.6)	5.0 (1.9–7.8)
Droplet number concentration ( $N_{\text{liq}}$ ), $\text{cm}^{-3}$	41 (12–525)	338 (188–782)

\*  $\text{CN}_{\text{PCASP}}$  equivalent data.**Table 8.** Mean properties and ranges for the 1 July 2008 ARCTAS case study, including background, intermediate, and biomass burning cloud cases.

Property	Background ( $n = 2$ )	Intermediate ( $n = 3$ )	Biomass burning ( $n = 2$ )
Aerosol number concentration ( $\text{CN}_{\text{PCASP}}^*$ ), $\text{cm}^{-3}$	249 (107–390)	294 (147–427)	2604 (2207–3001)
CCN, $\text{cm}^{-3}$	545 (205–592)	722 (462–908)	10 879 (10 348–11 411)
Backscatter at 550 nm, $\text{Mm}^{-1}$	1.7 (0.9–2.5)	3.3 (1.6–4.7)	35.7 (31.2–40.2)
Temperature, $^{\circ}\text{C}$	0.8 (0.2–0.9)	0.1 (–0.1 to 3.1)	2.8 (2.4–3.1)
Pressure, mbar	766 (762–770)	786 (763–826)	808
Liquid water content (LWC), $\text{g m}^{-3}$	0.07 (0.03–0.12)	0.02 (0.01–0.04)	0.01 (0.01–0.02)
Cloud droplet effective radius ( $r_e$ ), $\mu\text{m}$	4.8 (3.7–5.8)	2.6 (2.1–3.3)	1.9 (1.9–2.0)
Droplet number concentration ( $N_{\text{liq}}$ ), $\text{cm}^{-3}$	454 (384–525)	749 (621–907)	936 (824–1048)

\* Or  $\text{CN}_{\text{PCASP}}$  equivalent for ARCTAS data.

subjected to fresh concentrated smoke rather than aged diluted smoke, as one would expect at higher latitudes. Therefore, as explained above, we expect case study clouds already affected by high smoke concentrations to have reduced sensitivity to additional smoke, particularly given the low LWC of the case study clouds.

To assess the impact of smoke on liquid clouds more generally, we compared background and biomass burning cloud properties sampled over the larger region shown in Fig. 4. This more expansive set of clouds includes a broader range of high-latitude meteorological conditions, making it more representative of overall conditions in the Arctic region. However, the greater heterogeneity also makes trends in the data more difficult to interpret, as we cannot describe in full detail the degree to which meteorological influences affected each cloud given the limitations of the data sets.

Despite the uncertain meteorological influence, we see qualitatively similar trends to those in the 1 July 2008 ARCTAS case study (Fig. 7). We find a 3.7  $\mu\text{m}$  (42 %) median reduction in  $r_e$  between the smoky and background cases (Table 7). Concurrently, median  $N_{\text{liq}}$  increased from 41 droplets  $\text{cm}^{-3}$  in background clouds to 338 droplets  $\text{cm}^{-3}$  in smoky clouds. Within stratiform-only and cumuliform-only liquid clouds, groupings that are somewhat more comparable meteorologically, the mean  $r_e$  differences are 2.5 and

6.4  $\mu\text{m}$  ( $n = 13$  and 14), respectively. However, the combined median ACI estimate from all tracers shown in Fig. 7 is 0.16 (95 % confidence interval 0.14–0.17). This value is three times that of the case study, which is further evidence to suggest that cloud sensitivity to aerosols in the case study was lowered by aerosol-driven adiabatic reductions in cloud supersaturation (and possibly enhanced entrainment).

Observed smoke-driven reductions in liquid cloud droplet size and increases in cloud droplet number in both the case study and the multi-campaign analysis are in line with several other studies in the Arctic. Peng et al. (2002) found a similar difference in  $r_e$  of 4.8  $\mu\text{m}$  to the multi-campaign analysis in two combined data sets in the Arctic (one of which was the NRC FIRE.ACE data set), in conditions where PCASP values were  $>$  and  $<$  300 particles  $\text{cm}^{-3}$ , although they did not specifically focus on biomass-burning-related samples. Tietze et al. (2011) also found significant changes in LWP,  $\tau$ , and  $r_e$  using remote sensing cloud observations combined with a modeled biomass burning tracer. In contrast, Earle et al. (2011) did not see a reduction in  $r_e$  in biomass-burning-influenced clouds based on selected ISDAC samples. They attributed this finding to a combination of meteorological and microphysical factors. It is possible that some of the differences with our study are also caused by reduced contrast between selected clean and polluted cases, as their cutoff for

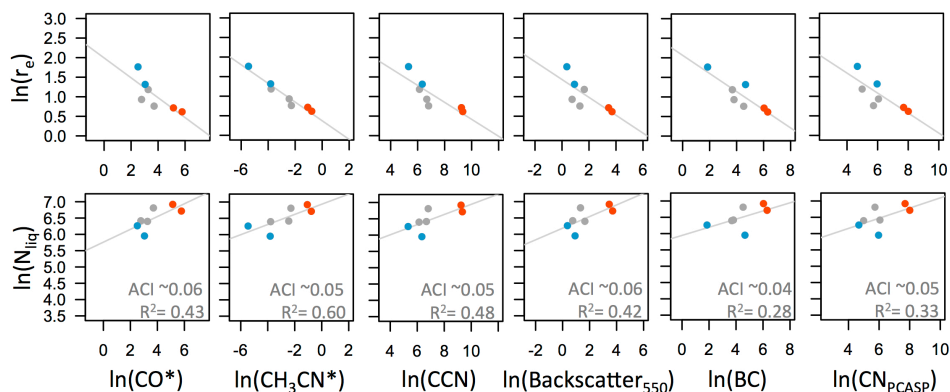


**Figure 5.** Based on seven samples from the ARCTAS-B 1 July 2008 case study, here we show the relationships between  $\ln(r_e)$  (top row) and  $\ln(N_{\text{liq}})$  (bottom row) and  $\ln(\text{BB}_t)$  derived from six indicators (where  $\text{BB}_t = \text{CO}$  (ppbv) ( $\times$  indicates background values of 99.2 ppbv have been subtracted),  $\text{CH}_3\text{CN}$  (ppbv) ( $\times$  indicates background values of 0.088 ppbv have been subtracted),  $\text{CCN}$  ( $\text{cm}^{-3}$ ), backscatter at 550 nm ( $\text{Mm}^{-1}$ ),  $\text{BC}$  ( $\mu\text{g C m}^{-3}$ ), and  $\text{CN}_{\text{PCASP}}$  equivalent values ( $\text{cm}^{-3}$ ), as calculated from UHSAS and APS measurements. Biomass burning samples are noted in red, and background samples are noted in blue. To show variation between tracers, linear regressions and associated ACI estimates are shown in light gray (but note that final ACI values are not derived from individual regressions, but rather a combination of all six tracers).

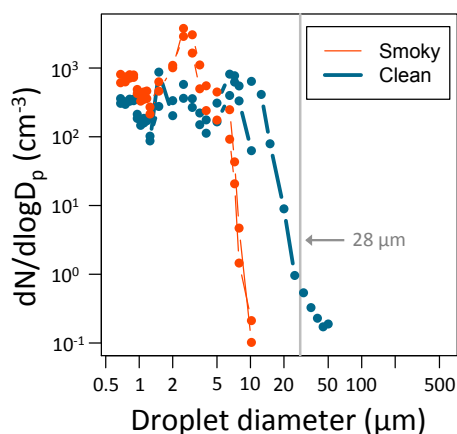


**Figure 6.** Mean cloud droplet size distributions ( $\mu\text{m}$ ) for individual case study biomass burning clouds (thin orange lines) and clean background clouds (thick blue lines). The  $28 \mu\text{m}$  line is marked in gray.

defining clean conditions was higher than ours, and they did not include any samples that met our background criteria (which were only present during the 4 April 2008 ISDAC flight). Also note that the biomass-burning-influenced cloud cases assessed by Earle et al. (2011) did not overlap with the clouds assessed in this study.

As noted previously, because the aircraft could only sample transects of clouds, we had to assume that the observed cloud phase was representative of the whole cloud. In the case study, all clouds were sampled at temperatures  $> 0^\circ\text{C}$ , and this assumption holds well. Where we expect this assumption to be most uncertain is in stratiform clouds in the multi-campaign analysis, which might have different proper-

ties in far-off, non-sampled portions. Uncertainties are also higher in clouds that were only transected horizontally, because mixed-phase clouds in the Arctic frequently have vertical layers of ice and liquid particles (Morrison et al., 2012). We cannot fully rule out that non-sampled portions of the clouds in the multi-campaign analysis contained ice particles, or that different vertical layers had different  $r_e$  values. However, if the six ISDAC and FIRE. ACE background clouds that were either stratiform or that contained only horizontal transects are excluded, the results of the multi-campaign analysis are nearly the same (ACI = 0.15 and median background cloud  $r_e = 7.0$  vs.  $7.6 \mu\text{m}$ ). Thus we do not believe that uncertainties in cloud phase had a major impact on our results.

### 3.2 Implications for radiation and precipitation

Based on model output by McComiskey and Feingold (2008) (their Fig. 2a), we estimate that given the case study median ACI value of 0.05, the smoke-derived cloud albedo effect on summertime local short-wave radiative forcing could be between  $-2$  and  $-4 \text{ W m}^{-2}$  for regions with surface albedo of  $\sim 0.15$ . Typical short-wave spectrum broadband (0.3–5.0  $\mu\text{m}$ ) albedos over subarctic Canada range from  $\sim 0.09$  to 0.17, compared to  $\sim 0.23$  to 0.71 in the winter (Davidson and Wang, 2005); thus, any local forcing in winter from smoke ACI effects would likely be reduced, compared to the summer. The McComiskey and Feingold (2008) output was also based on the assumption of homogeneous, unbroken clouds with  $\text{CCN}$  concentrations of  $600 \text{ cm}^{-3}$ , an LWP of  $50 \text{ g m}^{-2}$ , and a cloud base height of 500 m. Such surface albedo and cloud/aerosol conditions are similar to some of the summer terrestrial conditions sampled over Canada during ARCTAS-



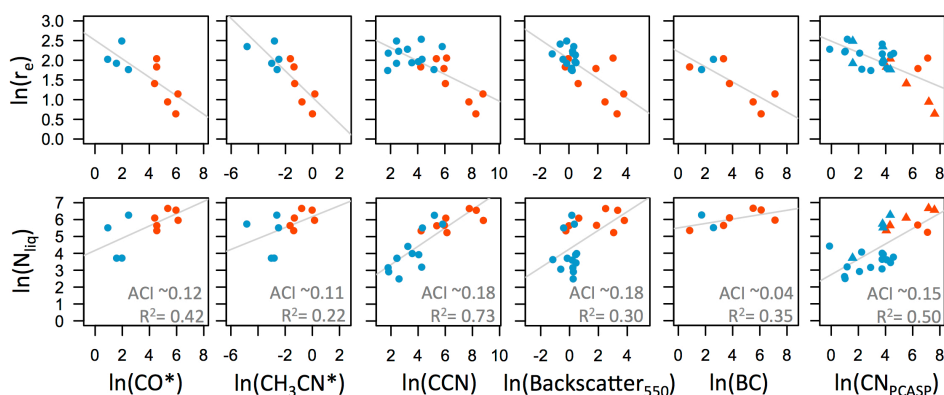


**Figure 7.** Same as in Fig. 5, but for data from the multi-campaign analysis. As in Fig. 5, CO\* indicates that background values of 99.2 ppbv have been subtracted. For CH<sub>3</sub>CN, the \* indicates background values of 0.018 ppbv have been subtracted (due to low background CH<sub>3</sub>CN levels in some of the samples).

B. The summer subarctic biomass burning clouds we describe from ARCTAS-B CCN and LWP levels bracket the model's assumptions, ranging between 1 and 94 g m<sup>-2</sup> and 68 and 6670 cm<sup>-3</sup>, respectively. However, cloud base heights were typically higher than the model-assumed 500 m, and although unbroken clouds are frequently observed in the Arctic and subarctic, the ACI value we use was determined from samples that included some clouds within broken cloud systems, which may possibly have different microphysical responses to aerosols. Periodic broken cloud conditions, cloud heterogeneity (McComiskey and Feingold, 2008), and the patchiness of smoke will all reduce the net cloud albedo radiative forcing over wider spaces and times. Therefore, the -2 to -4 W m<sup>-2</sup> range is only applicable in the subarctic in some summertime conditions. Nonetheless, this estimate at least provides a rough indication of how important these local effects might be during the most relevant time periods (i.e., when burning is most likely to occur).

In contrast to the subarctic, in the Arctic, high surface albedo will lessen the expected impact of the cloud albedo effect. Although future sea ice losses and associated reductions in surface albedo may affect the relative importance of the cloud albedo effect on Arctic clouds, others (e.g., Garret et al., 2004) have suggested that in the Arctic, a more important impact of reduced cloud droplet size may be greater long-wave opacity, which can lead to enhanced snowmelt. Relatedly, smaller droplets may affect cloud lifetime either by extending it via reduced precipitation (the “second indirect effect”; Ackerman et al., 2000; Albrecht, 1989) or by reducing it via enhanced water vapor competition and evaporation, as may have occurred in the case study.

Cloud droplet spectra from the 1 July 2008 ARCTAS case study clouds are shown in Fig. 6. Although sample size is small, the presence of smoke appears to narrow the droplet spectra from a dispersion of 0.84 in background clouds to 0.55 in smoky clouds, as calculated by the ratio between the standard deviation of the size distribution and the mean

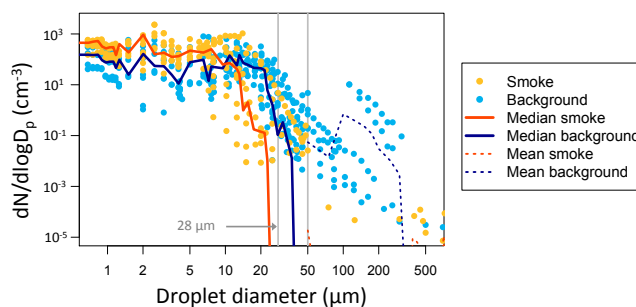


**Figure 8.** Mean cloud particle size distributions (μm) for all non-case study biomass burning clouds (yellow dots) and clean background clouds (light blue dots). The 28 and 50 μm lines are marked in gray. Thick red and darker blue lines indicate median values for binned size classes for smoky and clean clouds, respectively, including zero values not shown on the log–log plot. Due to the high number of zero values above > 50 μm diameter, the mean values above this level are also shown (dashed lines) for comparison.

droplet radius. This narrowing is likely to lessen the eventual probability of precipitation (Tao et al., 2012), as it moves median droplet size further away from the 28 μm effective diameter threshold at which collision/coagulation processes are thought to become efficient enough to induce precipitation (Rosenfeld et al., 2012).

Cloud droplet spectra from the multi-campaign clouds are shown for comparison in Fig. 8. There is not as obvious a narrowing of spectra as for the case study, but median droplet concentrations in smoky clouds never reached above 28+ μm diameter, whereas median droplet diameter in background clouds did reach above this point (Fig. 8). Also, small droplet concentrations (those most susceptible to evaporation) increased in smoky conditions, and rainfall was only noted in clean conditions, as shown in Fig. 8 by elevated (> 0.1 cm<sup>-3</sup>) cloud droplet concentrations with diameters > 50 μm (King et al., 2013). Therefore, although clouds outside the case

study suffer large uncertainties related to their collection over heterogeneous conditions, their droplet distributions support the hypothesis of smoke-induced reductions in drizzle.

### 3.3 Interactions of background aerosols with dilute biomass burning particles: a potential uncertainty in ACI values

As mentioned previously, large numbers of nucleation- and Aitken-mode particles are frequently observed in the spring and summer Arctic and subarctic (Engvall et al., 2008; Leck and Bigg, 1999; Ström et al., 2009; Zhao and Garrett, 2015). These particles are thought to have a marine origin via some combination of new particle formation from marine gases (Allan et al., 2015; Leaitch et al., 2013; O'Dowd et al., 2010; Tunved et al., 2013) and direct oceanic nanogel emissions (Heintzenberg et al., 2006; Karl et al., 2012, 2013; Leck and Bigg, 1999; Orellana et al., 2011). Chemical data from the ARCTAS data set also show the presence of numerous small particles with a natural background source (Fig. 9).

Previous studies also suggest that the small particles can condense upon larger particles (e.g., smoke) when such particles are present (Engvall et al., 2008; Leaitch et al., 2013; Tunved et al., 2013). This coagulation process may explain why Arctic smoke aerosols have been shown to sometimes contain organic components likely derived from smaller, non-biomass-burning particles mixed with sulfates and marine particles (Earle et al., 2011; Zelenyuk et al., 2010). To get some idea of how important the background particles may be, we estimated the maximum mean aerosol volume change that would occur if high concentrations of small background aerosols were to mix with and condense upon diluted smoke particles. Concentrations of background particles were estimated at  $5000\text{ cm}^{-3}$  (based on high-end values observed in Fig. 9 and at another Arctic site; Ström et al., 2009). Diluted smoke concentrations were estimated at  $450\text{ particles cm}^{-3}$  (low-end values from Fig. 9). Volumes were calculated from the size ranges observed in ARCTAS background and smoky aerosols (see Appendix A for details). In this hypothetical scenario, we estimate that background aerosols could increase dilute smoke aerosol volume by up to 2–15%, although volume increases are likely substantially less in most air masses.

Interestingly, the small Arctic marine particles appear to be fairly hygroscopic (Latham et al., 2013; Lawler et al., 2014; Zhou et al., 2001), and they can be surface-active (Lohmann and Leck, 2005). One study using ARCTAS data showed that background aerosol values of the hygroscopicity parameter,  $\kappa$ , were on average nearly 2 times higher than average smoke  $\kappa$  values ( $0.32 \pm 0.21$  vs.  $0.18 \pm 0.13$ , respectively), although there was a high degree of variability and overlap in the  $\kappa$  values (Latham et al., 2013). Previous studies also suggest that volume increases alone might affect Arctic particle hygroscopicity, independent of chemistry (Moore et al., 2011). Given this information, we cannot rule out that

upon condensation, the small background particles might act as surfactants or otherwise modify smoke CCN characteristics, causing deviations from the ACI value as derived in Sect. 3.1 at low smoke concentrations. This hypothesis is difficult to test because, excepting three intermediate instances in the case study, the data presented in Sect. 3.2 only included background and high smoke conditions.

However, the nucleation- and Aitken-mode background particles are not ubiquitous throughout the year. They tend to accumulate mainly in the spring and summer, which is thought to be due to a combination of three factors: (1) there is more sunlight available for the photochemical reactions key to new particle formation (Engvall et al., 2008; Tunved et al., 2013), (2) reduced sea ice and enhanced primary production likely lead to greater emissions of marine precursor gases and nanogels (Leaitch et al., 2013; O'Dowd et al., 2010; Tunved et al., 2013), and (3) during Arctic summer there tend to be fewer larger particles such as smoke for these small particles to coagulate and condense upon. However, Arctic summertime smoke events do occur (e.g., Fuelberg et al., 2010; Iziomon et al., 2006) and may be increasing (Moritz et al., 2012). In the subarctic, wildfires peak in the summer (Giglio et al., 2006). Thus, although the influence of the small background particles on subarctic and Arctic smoke ACI values is probably minor, deviations from the linear ACI expectations derived here might occur during dilute summertime Arctic smoke events and in subarctic locations, for example when smoke is diluted over or near marine environments.

## 4 Discussion and conclusions

The challenge of separating the influence of meteorology and aerosol indirect effects on clouds introduces relatively large uncertainty in our understanding of how smoke impacts clouds. Using in situ aircraft data, we quantified these impacts in both a subarctic cumulus cloud case study and in a multi-campaign data assessment of clouds north of  $50^\circ\text{N}$ . The multi-campaign assessment suggests an ACI value of 0.16 (95% confidence interval 0.10–0.13), which is on the high end of previous satellite-based assessments (0.04–0.11) (Tietze et al., 2011). Given a known low bias in remote-sensing-derived estimates of ACIs (e.g., McComiskey and Feingold, 2012), our findings suggest that smoke-derived increases in cloud albedo may be higher than previously derived in the region. We reduced confounding meteorological effects by including data from as wide a geographic region as possible, applying very stringent conditions to identify clean and smoky clouds, and reducing the impact of outliers on ACI derivations by using the Kendall robust line-fit method instead of normal linear regressions. However it is important to note that meteorological effects are still imperfectly constrained in this assessment due to inherent limitations in the in situ data set size and content.

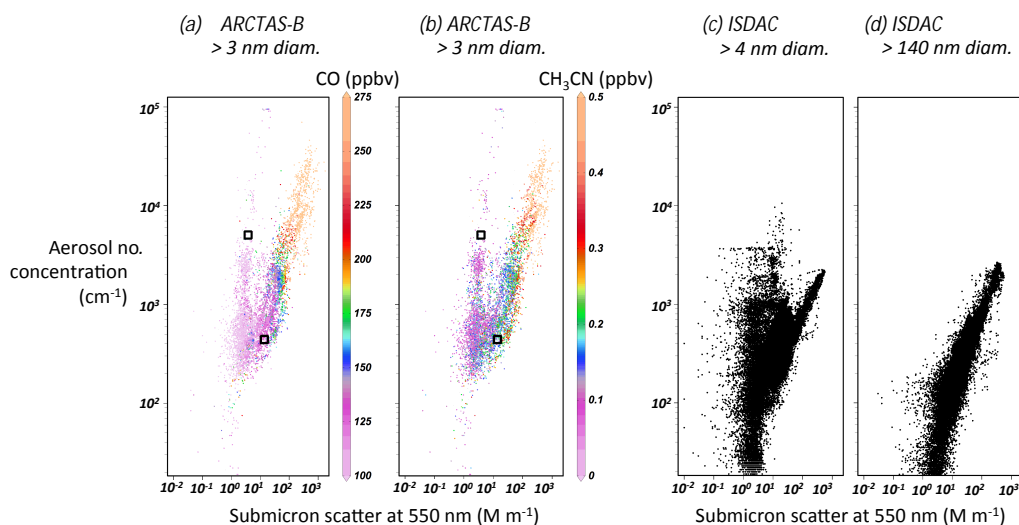


**Figure 9.** Log relationships between ARCTAS-B and ISDAC aerosol number concentration and submicron scatter. In panels (a) and (b), the combustion tracer, CO, and the biomass burning tracer, CH<sub>3</sub>CN, are also shown in out-of-cloud air masses. The black squares in panels (a) and (b) indicate where background aerosol concentrations of 5000 cm<sup>-3</sup> and dilute smoke concentrations of 450 cm<sup>-3</sup> would be relative to other points. Measurements are from the following instruments: (a) and (b) TSI 3025, (c) TSI 3775, and (d) PCASP. ARCTAS-B summertime samples were taken at altitudes < 5.2 km; ISDAC samples were taken at < 3.65 km due to TSI3025 instrument limitations. All quality-flagged data were excluded, as well as suspicious ISDAC values within 17 km and < 1 km altitude of Fairbanks airport, Alaska. Very small background aerosols appear to dominate the high aerosol number concentration/low scatter particles seen in (a)–(c), as shown by their disappearance when a diameter cutoff of 140 nm is used (d).

For comparison to the multi-campaign analysis, we also analyzed the 1 July 2008 ARCTAS case in the subarctic, where multiple clean and smoky clouds were found under similar meteorological conditions. The case study smoke cases had a combination of low cloud LWC, high in-plume aerosol concentrations, and very small cloud droplets. From these samples, we derived an ACI estimate of 0.05 (95 % confidence interval 0.04–0.06), which is smaller than that of the multi-campaign analysis. Based on theory (e.g., Moore et al., 2013), as the number of smoke CCN increases (through some combination of enhanced aerosol number and/or increased hygroscopicity for existing particles), there is greater water vapor competition. This competition makes supersaturation development and cloud droplet activation increasingly difficult, which would reduce ACI values. Therefore, we speculate that the 0.05 ACI case study value falls at the low-end of typical smoke ACI values for the larger subarctic/Arctic region. Reductions in droplet activation and potential enhanced evaporation would also limit the maximum magnitude of smoke cloud albedo effects.

Based on a previous model study by McComiskey and Feingold (2008), the ACI value of 0.05 from the case study suggests that smoke may reduce local summertime radiative flux via the cloud albedo effect by between 2 and 4 W m<sup>-2</sup> or more under low and homogeneous cloud cover conditions in the subarctic. At higher latitudes where surface albedo is already high, the impact on radiative flux is likely to be smaller. In those regions, a more important effect of smoke might be

its inhibition of precipitation and cloud lifetime effect, as evidenced by the observed reductions in cloud droplet radius of ~ 50 % in both the case study and the multi-campaign assessment.

Smaller cloud droplets can have various consequences. Smoke-driven reductions or delays in precipitation may affect the distribution of aerosol and moisture deposition. Longer cloud lifetime could impact not only Arctic albedo but also long-wave radiation (Stone, 1997), and previous studies suggest that even small changes in the above parameters may affect sensitive Arctic sea ice (Kay et al., 2008; Kay and Gettelman, 2009; Lubin and Vogelmann, 2006; Vavrus et al., 2010). Additionally, changes in cloud cover might also have indirect effects on ocean photosynthesis and biogeochemistry (Bélanger et al., 2013). It is our hope that the improved quantification of smoke-derived ACI values will help quantify these impacts in future model studies.

One obvious limitation of our study is that we do not address the impacts of smoke on existing mixed- and ice-phase clouds. Additionally, we cannot account for the ways in which smoke might have affected the sample phase. For example, ice nuclei presence might facilitate the conversion of an otherwise liquid-phase cloud into a mixed-phase cloud that was excluded in this assessment. Alternatively, we could have included liquid clouds in our assessment that might otherwise have been present as mixed- or ice-phase clouds if not for the inhibition of freezing by soluble smoke compounds via the Raoult effect (discussed in Tao et al., 2012).



Finally, we have presented evidence to suggest that coagulation of the numerous nucleation- and Aitken-mode background particles frequently present in clean summertime Arctic air masses might increase the volume of diluted smoke aerosols by up to 2–15 %. Previous studies suggest that such interactions with background particles may increase smoke aerosol hygroscopicity, which in turn could cause deviations

from the ACI value derived here. Future remote sensing or ground-based analyses may be able to more completely address the different impacts of dilute vs. concentrated smoke aerosols in Arctic clouds.

### Appendix A: Calculations for maximum potential contribution of background aerosol to diluted smoke aerosol volume

We first estimate the volume of smoke particles at dilute concentrations of  $450 \text{ particles cm}^{-3}$ . Arctic/subarctic smoke aerosol size distributions were taken from Kondo et al. (2011) and Sakamoto et al. (2015), where log-normal aerosol size distributions were characterized by geometric mean diameters of  $224 \pm 14$  and  $230 \text{ nm}$  and geometric standard deviations of  $1.33 \pm 0.05$  and  $1.5$ , respectively. From the corresponding size distributions, we estimate smoke aerosol volumes of  $\sim 2.9\text{--}6.0 \mu\text{m}^3 \text{ per cm}^{-3}$  of air at smoke concentrations of  $450 \text{ cm}^{-3}$ .

The degree to which aerosol properties can be affected by the collection of Arctic nucleation- and Aitken-mode background particles onto larger smoke and pollution particles also depends in part on the size ranges and concentrations of the background particles. These can be quite variable (Engvall et al., 2008) (also see Fig. A1). To estimate average background concentrations, we use the observed geometric mean ratio range in 6-year Svalbard summertime data (Engvall et al., 2008), which indicated that Aitken-mode particle concentrations were  $\sim 1.5\text{--}3$  times greater than those of accumulation-mode particles. Given this range in ratios, we would expect background particle concentrations to be  $\sim 675\text{--}1350 \text{ cm}^{-3}$  at smoke concentrations of  $450 \text{ cm}^{-3}$ . We then combine the expected small background aerosol concentrations with ARCTAS background aerosol spectra from events from 12 April, 10 July, and 13 July 2008 (Fig. A1) for particles  $< 80 \text{ nm}$  in diameter. Based on these values, the small background aerosol volume is estimated at  $0.012\text{--}0.114 \mu\text{m}^3 \text{ cm}^{-3}$ . A comparison of this volume with the previously estimated smoke aerosol volume suggests that background aerosols could contribute only  $\sim 0.2\text{--}4\%$  of total diluted smoke aerosol volume in average summertime conditions. This estimate does not account for the fact that all else being equal, small particles are usually more likely to coagulate onto the largest sized particles (Seinfeld and Pandis, 1998), which would reduce the contribution to average particle volume even further.

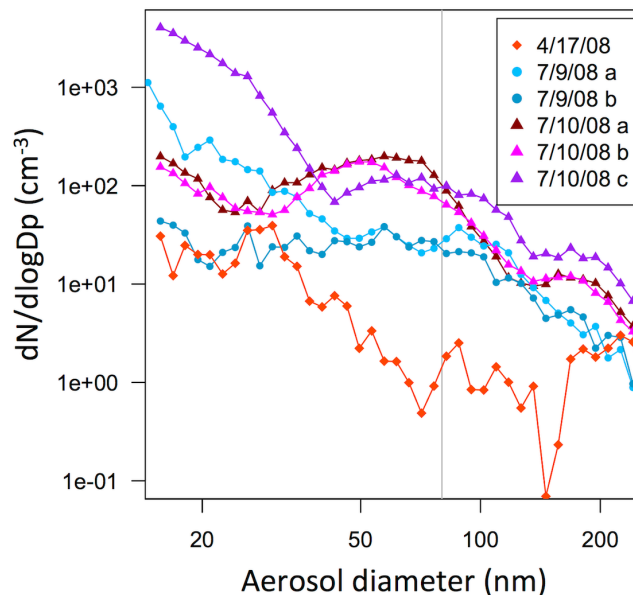


**Figure A1.** Mean out-of-cloud aerosol particle size distributions for several ARCTAS background aerosol events. Some days had multiple background aerosol events; these are distinguished by color and the letters (a)–(c). The light gray line shows the  $80 \text{ nm}$  cutoff used here to distinguish Aitken-mode particles from accumulation-mode particles.

Alternatively, we can estimate what the background aerosol volume might be if particle concentrations were as high as  $5000 \text{ cm}^{-3}$ . Although such events are not common in the Arctic and subarctic, similar high-end concentrations of background particles are observed in Fig. 9 and have been observed elsewhere in the Arctic as well (Ström et al., 2009). Again assuming the same range of particle size distributions observed in Fig. A1, the small background aerosol volume at  $5000 \text{ particles cm}^{-3}$  is estimated to be between  $0.092$  and  $0.422 \mu\text{m}^3 \text{ per cm}^{-3}$  of air. Thus, in this case, background aerosols could add at most  $2\text{--}15\%$  of total aerosol volume in diluted smoke with concentrations of  $450 \text{ particles cm}^{-3}$ .

**Acknowledgements.** The authors would like to thank A. Aknan, B. Anderson, E. Apel, G. Chen, M. Couture, T. Garrett, K. B. Huebert, A. Khain, A. Korolev, T. Latham, P. Lawson, R. Leaitch, J. Limbacher, J. Nelson, M. Pinsky, W. Ridgeway, A. Rangno, S. Williams, S. Woods, and Y. Yang for data and/or advice or help with various aspects of this project, and all others who were involved in collecting and funding the collection of the data sets we have used. We acknowledge the Atmospheric Radiation Measurement (ARM) Program sponsored by the U.S. Department of Energy, Office of Science, Office of Biological and Environmental Research, Climate and Environmental Sciences Division for providing the ISDAC data set. The authors also gratefully acknowledge the NOAA Air Resources Laboratory (ARL) for the provision of the HYSPLIT transport and dispersion model and/or READY website (<http://www.ready.noaa.gov>) used in this publication. Plots were made with Ocean Data View (Schlitzer, R., Ocean Data View, <http://odv.awi.de>, 2015) and R (R Core Team, 2013). CH<sub>3</sub>CN measurements were supported by the Austrian Federal Ministry for Transport, Innovation and Technology (bmvit) through the Austrian Space Applications Programme (ASAP) of the Austrian Research Promotion Agency (FFG). T. Mikoviny is acknowledged for his support with the CH<sub>3</sub>CN data acquisition and analysis. LMZ's funding for this study was provided by an appointment to the NASA Postdoctoral Program at Goddard Space Flight Center, administered by Oak Ridge Associated Universities through a contract with NASA. M. J. Cubison and J. L. Jimenez were supported by NASA NNX12AC03G and NNX15AH33A.

Edited by: L. M. Russell

## References

- Ackerman, A. S., Toon, O. B., Stevens, D. E., Heymsfield, A. J., Ramanathan, V., and Welton, E. J.: Reduction of Tropical Cloudiness by Soot, *Science*, 288, 1042–1047, doi:10.1126/science.288.5468.1042, 2000.
- Ackerman, A. S., Kirkpatrick, M. P., Stevens, D. E., and Toon, O. B.: The impact of humidity above stratiform clouds on indirect aerosol climate forcing, *Nature*, 432, 1014–1017, doi:10.1038/nature03174, 2004.
- Albrecht, B. A.: Aerosols, Cloud Microphysics, and Fractional Cloudiness, *Science*, 245, 1227–1230, doi:10.1126/science.245.4923.1227, 1989.
- Allan, J. D., Williams, P. I., Najera, J., Whitehead, J. D., Flynn, M. J., Taylor, J. W., Liu, D., Darbyshire, E., Carpenter, L. J., Chance, R., Andrews, S. J., Hackenberg, S. C., and McFiggans, G.: Iodine observed in new particle formation events in the Arctic atmosphere during ACCACIA, *Atmos. Chem. Phys.*, 15, 5599–5609, doi:10.5194/acp-15-5599-2015, 2015.
- Alvarado, M. J., Logan, J. A., Mao, J., Apel, E., Riemer, D., Blake, D., Cohen, R. C., Min, K.-E., Perring, A. E., Browne, E. C., Wooldridge, P. J., Diskin, G. S., Sachse, G. W., Fuelberg, H., Sessions, W. R., Harrigan, D. L., Huey, G., Liao, J., Case-Hanks, A., Jimenez, J. L., Cubison, M. J., Vay, S. A., Weinheimer, A. J., Knapp, D. J., Montzka, D. D., Flocke, F. M., Pollack, I. B., Wennberg, P. O., Kurten, A., Crouse, J., Clair, J. M. St., Wisthaler, A., Mikoviny, T., Yantosca, R. M., Carouge, C. C., and Le Sager, P.: Nitrogen oxides and PAN in plumes from boreal fires during ARCTAS-B and their impact on ozone: an integrated analysis of aircraft and satellite observations, *Atmos. Chem. Phys.*, 10, 9739–9760, doi:10.5194/acp-10-9739-2010, 2010.
- Balshi, M. S., Mcguire, A. D., Duffy, P., Flannigan, M., Kicklighter, D. W., and Melillo, J.: Vulnerability of carbon storage in North American boreal forests to wildfires during the 21st century, *Glob. Change Biol.*, 15, 1491–1510, doi:10.1111/j.1365-2486.2009.01877.x, 2009.
- Baum, B. A., Menzel, W. P., Frey, R. A., Tobin, D. C., Holz, R. E., Ackerman, S. A., Heidinger, A. K., and Yang, P.: MODIS Cloud-Top Property Refinements for Collection 6, *J. Appl. Meteorol. Climatol.*, 51, 1145–1163, doi:10.1175/JAMC-D-11-0203.1, 2012.
- Baumgardner, D.: An analysis and comparison of five water droplet measuring instruments, *J. Appl. Meteor.*, 22, 891–910, doi:10.1175/1520-0450(1983)022<0891:AAACOF>2.0.CO;2, 1983.
- Baumgardner, D., Jonsson, H., Dawson, W., O'Connor, D., and Newton, R.: The cloud, aerosol and precipitation spectrometer: a new instrument for cloud investigations, *Atmos. Res.*, 59–60, 251–264, doi:10.1016/S0169-8095(01)00119-3, 2001.
- Bélanger, S., Babin, M., and Tremblay, J.-É.: Increasing cloudiness in Arctic dampens the increase in phytoplankton primary production due to sea ice receding, *Biogeosciences*, 10, 4087–4101, doi:10.5194/bg-10-4087-2013, 2013.
- Bian, H., Colarco, P. R., Chin, M., Chen, G., Rodriguez, J. M., Liang, Q., Blake, D., Chu, D. A., da Silva, A., Darmenov, A. S., Diskin, G., Fuelberg, H. E., Huey, G., Kondo, Y., Nielsen, J. E., Pan, X., and Wisthaler, A.: Source attributions of pollution to the Western Arctic during the NASA ARCTAS field campaign, *Atmos. Chem. Phys.*, 13, 4707–4721, doi:10.5194/acp-13-4707-2013, 2013.
- Bretherton, C. S., Blossey, P. N., and Uchida, J.: Cloud droplet sedimentation, entrainment efficiency, and subtropical stratocumulus albedo, *Geophys. Res. Lett.*, 34, L03813, doi:10.1029/2006GL027648, 2007.
- Brock, C. A., Cozic, J., Bahreini, R., Froyd, K. D., Middlebrook, A. M., McComiskey, A., Brioude, J., Cooper, O. R., Stohl, A., Aikin, K. C., de Gouw, J. A., Fahey, D. W., Ferrare, R. A., Gao, R.-S., Gore, W., Holloway, J. S., Hübler, G., Jefferson, A., Lack, D. A., Lance, S., Moore, R. H., Murphy, D. M., Nenes, A., Novelli, P. C., Nowak, J. B., Ogren, J. A., Peischl, J., Pierce, R. B., Pilewskie, P., Quinn, P. K., Ryerson, T. B., Schmidt, K. S., Schwarz, J. P., Sodemann, H., Spackman, J. R., Stark, H., Thomson, D. S., Thornberry, T., Veres, P., Watts, L. A., Warneke, C., and Wollny, A. G.: Characteristics, sources, and transport of aerosols measured in spring 2008 during the aerosol, radiation, and cloud processes affecting Arctic Climate (ARCPAC) Project, *Atmos. Chem. Phys.*, 11, 2423–2453, doi:10.5194/acp-11-2423-2011, 2011.
- Cai, Y., Montague, D. C., Mooiweer-Bryan, W., and Deshler, T.: Performance characteristics of the ultra high sensitivity aerosol spectrometer for particles between 55 and 800 nm: Laboratory and field studies, *J. Aerosol Sci.*, 39, 759–769, doi:10.1016/j.jaerosci.2008.04.007, 2008.
- Chen, Y.-C., Christensen, M. W., Xue, L., Sorooshian, A., Stephens, G. L., Rasmussen, R. M., and Seinfeld, J. H.: Occurrence of lower cloud albedo in ship tracks, *Atmos. Chem. Phys.*, 12, 8223–8235, doi:10.5194/acp-12-8223-2012, 2012.

- Colman, J. J., Swanson, A. L., Meinardi, S., Sive, B. C., Blake, D. R., and Rowland, F. S.: Description of the Analysis of a Wide Range of Volatile Organic Compounds in Whole Air Samples Collected during PEM-Tropics A and B, *Anal. Chem.*, 73, 3723–3731, doi:10.1021/ac010027g, 2001.
- Costantino, L. and Bréon, F.-M.: Analysis of aerosol-cloud interaction from multi-sensor satellite observations, *Geophys. Res. Lett.*, 37, L11801, doi:10.1029/2009GL041828, 2010.
- Cubison, M. J., Ortega, A. M., Hayes, P. L., Farmer, D. K., Day, D., Lechner, M. J., Brune, W. H., Apel, E., Diskin, G. S., Fisher, J. A., Fuelberg, H. E., Hecobian, A., Knapp, D. J., Mikoviny, T., Riemer, D., Sachse, G. W., Sessions, W., Weber, R. J., Weinheimer, A. J., Wisthaler, A., and Jimenez, J. L.: Effects of aging on organic aerosol from open biomass burning smoke in aircraft and laboratory studies, *Atmos. Chem. Phys.*, 11, 12049–12064, doi:10.5194/acp-11-12049-2011, 2011.
- Curry, J. A., Hobbs, P. V., King, M. D., Randall, D. A., Minnis, P., Isaac, G. A., Pinto, J. O., Uttal, T., Bucholtz, A., Cripe, D. G., Gerber, H., Fairall, C. W., Garrett, T. J., Hudson, J., Intrieri, J. M., Jakob, C., Jensen, T., Lawson, P., Marcotte, D., Nguyen, L., Pilewskie, P., Rangno, A., Rogers, D. C., Strawbridge, K. B., Valero, F. P. J., Williams, A. G., and Wylie, D.: FIRE Arctic Clouds Experiment, *B. Am. Meteorol. Soc.*, 81, 5–29, doi:10.1175/1520-0477(2000)081<0005:FACE>2.3.CO;2, 2000.
- Davidson, A. and Wang, S.: Spatiotemporal variations in land surface albedo across Canada from MODIS observations, *Can. J. Remote Sens.*, 31, 377–390, doi:10.5589/m05-021, 2005.
- DeCarlo, P. F., Dunlea, E. J., Kimmel, J. R., Aiken, A. C., Sueper, D., Crouse, J., Wennberg, P. O., Emmons, L., Shinzuka, Y., Clarke, A., Zhou, J., Tomlinson, J., Collins, D. R., Knapp, D., Weinheimer, A. J., Montzka, D. D., Campos, T., and Jimenez, J. L.: Fast airborne aerosol size and chemistry measurements above Mexico City and Central Mexico during the MILAGRO campaign, *Atmos. Chem. Phys.*, 8, 4027–4048, doi:10.5194/acp-8-4027-2008, 2008.
- De Gouw, J. A., Warneke, C., Parrish, D. D., Holloway, J. S., Trainer, M., and Fehsenfeld, F. C.: Emission sources and ocean uptake of acetonitrile (CH<sub>3</sub>CN) in the atmosphere, *J. Geophys. Res.-Atmos.*, 108, 4329, doi:10.1029/2002JD002897, 2003.
- Duong, H. T., Sorooshian, A., and Feingold, G.: Investigating potential biases in observed and modeled metrics of aerosol-cloud-precipitation interactions, *Atmos. Chem. Phys.*, 11, 4027–4037, doi:10.5194/acp-11-4027-2011, 2011.
- Earle, M. E., Liu, P. S. K., Strapp, J. W., Zelenyuk, A., Imre, D., McFarquhar, G. M., Shantz, N. C., and Leaitch, W. R.: Factors influencing the microphysics and radiative properties of liquid-dominated Arctic clouds: Insight from observations of aerosol and clouds during ISDAC, *J. Geophys. Res.*, 116, D00T09, doi:10.1029/2011JD015887, 2011.
- Engvall, A.-C., Krejci, R., Ström, J., Treffeisen, R., Scheele, R., Hermansen, O., and Paatero, J.: Changes in aerosol properties during spring-summer period in the Arctic troposphere, *Atmos. Chem. Phys.*, 8, 445–462, doi:10.5194/acp-8-445-2008, 2008.
- Feingold, G., Remer, L. A., Ramaprasad, J., and Kaufman, Y. J.: Analysis of smoke impact on clouds in Brazilian biomass burning regions: An extension of Twomey's approach, *J. Geophys. Res.-Atmos.*, 106, 22907–22922, doi:10.1029/2001JD000732, 2001.
- Feingold, G., Eberhard, W. L., Veron, D. E., and Previdi, M.: First measurements of the Twomey indirect effect using ground-based remote sensors, *Geophys. Res. Lett.*, 30, 1287, doi:10.1029/2002GL016633, 2003.
- Fisher, J. A., Jacob, D. J., Wang, Q., Bahreini, R., Carouge, C. C., Cubison, M. J., Dibb, J. E., Diehl, T., Jimenez, J. L., Leibensperger, E. M., Lu, Z., Meinders, M. B. J., Pye, H. O. T., Quinn, P. K., Sharma, S., Streets, D. G., van Donkelaar, A., and Yantosca, R. M.: Sources, distribution, and acidity of sulfate-ammonium aerosol in the Arctic in winter-spring, *Atmos. Environ.*, 45, 7301–7318, doi:10.1016/j.atmosenv.2011.08.030, 2011.
- Flannigan, M. D., Krawchuk, M. A., de Groot, W. J., Wotton, B. M., and Gowman, L. M.: Implications of changing climate for global wildland fire, *Int. J. Wildland Fire*, 18, 483–507, 2009.
- Fuelberg, H. E., Harrigan, D. L., and Sessions, W.: A meteorological overview of the ARCTAS 2008 mission, *Atmos. Chem. Phys.*, 10, 817–842, doi:10.5194/acp-10-817-2010, 2010.
- Garrett, T. J. and Hobbs, P. V.: Calibration of liquid water probes from the University of Washington's CV-580 aircraft at the Canadian NRC wind tunnel, in *Rep. Cloud and Aerosol Research Group*, 20 pp., Dep. of Atmos. Sci, Univ. of Washington, Seattle, 1999.
- Garrett, T. J., Zhao, C., Dong, X., Mace, G. G., and Hobbs, P. V.: Effects of varying aerosol regimes on low-level Arctic stratus, *Geophys. Res. Lett.*, 31, L17105, doi:10.1029/2004GL019928, 2004.
- Gerber, H., Arends, B. G., and Ackerman A. S.: New microphysics sensor for aircraft use, *Atmos. Res.*, 31, 235–252, doi:10.1016/0169-8095(94)90001-9, 1994.
- Giglio, L., Csiszar, I., and Justice, C. O.: Global distribution and seasonality of active fires as observed with the Terra and Aqua Moderate Resolution Imaging Spectroradiometer (MODIS) sensors, *J. Geophys. Res.-Biogeosci.*, 111, G02016, doi:10.1029/2005JG000142, 2006.
- Hansen, J. E. and Travis, L. D.: Light scattering in planetary atmospheres, *Space Sci. Rev.*, 16, 527–610, doi:10.1007/BF00168069, 1974.
- Hecobian, A., Liu, Z., Hennigan, C. J., Huey, L. G., Jimenez, J. L., Cubison, M. J., Vay, S., Diskin, G. S., Sachse, G. W., Wisthaler, A., Mikoviny, T., Weinheimer, A. J., Liao, J., Knapp, D. J., Wennberg, P. O., Kürten, A., Crouse, J. D., Clair, J. St., Wang, Y., and Weber, R. J.: Comparison of chemical characteristics of 495 biomass burning plumes intercepted by the NASA DC-8 aircraft during the ARCTAS/CARB-2008 field campaign, *Atmos. Chem. Phys.*, 11, 13325–13337, doi:10.5194/acp-11-13325-2011, 2011.
- Hegg, D. A., Nielsen, K., Covert, D. S., Jonsson, H. H., and Durkee, P. A.: Factors influencing the mesoscale variations in marine stratocumulus albedo, *Tellus B*, 59, 66–76, doi:10.3402/tellusb.v59i1.16970, 2007.
- Hegg, D. A., Warren, S. G., Grenfell, T. C., Doherty, S. J., Larson, T. V., and Clarke, A. D.: Source Attribution of Black Carbon in Arctic Snow, *Environ. Sci. Technol.*, 43, 4016–4021, doi:10.1021/es803623f, 2009.
- Hegg, D. A., Warren, S. G., Grenfell, T. C., Doherty, S. J., and Clarke, A. D.: Sources of light-absorbing aerosol in arctic snow and their seasonal variation, *Atmos. Chem. Phys.*, 10, 10923–10938, doi:10.5194/acp-10-10923-2010, 2010.

- Heintzenberg, J., Leck, C., Birmili, W., Wehner, B., Tjernström, M., and Wiedensohler, A.: Aerosol number–size distributions during clear and fog periods in the summer high Arctic: 1991, 1996 and 2001, *Tellus B*, 58, 41–50, doi:10.1111/j.1600-0889.2005.00171.x, 2006.
- Howell, S. G., Clarke, A. D., Freitag, S., McNaughton, C. S., Kapustin, V., Brekovskikh, V., Jimenez, J.-L., and Cubison, M. J.: An airborne assessment of atmospheric particulate emissions from the processing of Athabasca oil sands, *Atmos. Chem. Phys.*, 14, 5073–5087, doi:10.5194/acp-14-5073-2014, 2014.
- Huffman, J., Jayne, J., Drewnick, F., Aiken, A., Onasch, T., Worsnop, D. and Jimenez, J.: Design, Modeling, Optimization, and Experimental Tests of a Particle Beam Width Probe for the Aerodyne Aerosol Mass Spectrometer, *Aerosol Sci. Technol.*, 39, 1143–1163, doi:10.1080/02786820500423782, 2005.
- Intrieri, J. M., Shupe, M. D., Uttal, T., and McCarty, B. J.: An annual cycle of Arctic cloud characteristics observed by radar and lidar at SHEBA, *J. Geophys. Res. Oceans*, 107, SHE 5–1, doi:10.1029/2000JC000423, 2002.
- Iziomon, M. G., Lohmann, U., and Quinn, P. K.: Summertime pollution events in the Arctic and potential implications, *J. Geophys. Res.*, 111, D12206, doi:10.1029/2005JD006223, 2006.
- Jackson, R. C., McFarquhar, G. M., Korolev, A. V., Earle, M. E., Liu, P. S. K., Lawson, R. P., Brooks, S., Wolde, M., Laskin, A., and Freer, M.: The dependence of ice microphysics on aerosol concentration in arctic mixed-phase stratus clouds during ISDAC and M-PACE, *J. Geophys. Res.*, 117, D15207, doi:10.1029/2012JD017668, 2012.
- Jacob, D. J., Crawford, J. H., Maring, H., Clarke, A. D., Dibb, J. E., Emmons, L. K., Ferrare, R. A., Hostetler, C. A., Russell, P. B., Singh, H. B., Thompson, A. M., Shaw, G. E., McCauley, E., Pederson, J. R., and Fisher, J. A.: The Arctic Research of the Composition of the Troposphere from Aircraft and Satellites (ARCTAS) mission: design, execution, and first results, *Atmos. Chem. Phys.*, 10, 5191–5212, doi:10.5194/acp-10-5191-2010, 2010.
- Jouan, C., Girard, E., Pelon, J., Gultepe, I., Delanoë, J., and Blanchet, J.-P.: Characterization of Arctic ice cloud properties observed during ISDAC, *J. Geophys. Res. Atmos.*, 117, D23207, doi:10.1029/2012JD017889, 2012.
- Karl, M., Leck, C., Gross, A., and Pirjola, L.: A study of new particle formation in the marine boundary layer over the central Arctic ocean using a flexible multicomponent aerosol dynamic model, *Tellus*, 64B, 17158, doi:10.3402/tellusb.v64i0.17158, 2012.
- Karl, M., Leck, C., Coz, E., and Heintzenberg, J.: Marine nanogels as a source of atmospheric nanoparticles in the high Arctic, *Geophys. Res. Lett.*, 40, 3738–3743, doi:10.1002/grl.50661, 2013.
- Kay, J. E. and Gettelman, A.: Cloud influence on and response to seasonal Arctic sea ice loss, *J. Geophys. Res.*, 114, D18204, doi:10.1029/2009JD011773, 2009.
- Kay, J. E., Ecuyer, T. L., Gettelman, A., Stephens, G., and O'Dell, C.: The contribution of cloud and radiation anomalies to the 2007 Arctic sea ice extent minimum, *Geophys. Res. Lett.*, 35, L08503, doi:10.1029/2008GL033451, 2008.
- King, W. D., Parkin D. A., and Handsworth R. J.: A hot-wire water device having fully calculable response characteristics, *J. Appl. Meteor.*, 17, 1809–1813, doi:10.1175/1520-0450(1978)017<1809:AHWLWD>2.0.CO;2, 1978.
- King, N. J., Bower, K. N., Crosier, J., and Crawford, I.: Evaluating MODIS cloud retrievals with in situ observations from VOCALS-REx, *Atmos. Chem. Phys.*, 13, 191–209, doi:10.5194/acp-13-191-2013, 2013.
- Kondo, Y., Matsui, H., Moteki, N., Sahu, L., Takegawa, N., Kajino, M., Zhao, Y., Cubison, M. J., Jimenez, J. L., Vay, S., Diskin, G. S., Anderson, B., Wisthaler, A., Mikoviny, T., Fuelberg, H. E., Blake, D. R., Huey, G., Weinheimer, A. J., Knapp, D. J., and Brune, W. H.: Emissions of black carbon, organic, and inorganic aerosols from biomass burning in North America and Asia in 2008, *J. Geophys. Res.-Atmos.*, 116, D08204, doi:10.1029/2010JD015152, 2011.
- Korolev, A. V., Strapp, J. W., Isaac, G. A., and Nevzorov, A. N.: The Nevzorov Airborne Hot-Wire LWC–TWC Probe: Principle of Operation and Performance Characteristics, *J. Atmos. Ocean. Technol.*, 15, 1495–1510, doi:10.1175/1520-0426(1998)015<1495:TNAHWL>2.0.CO;2, 1998.
- Korolev, A. V., Isaac, G. A., Cober, S. G., Strapp, J. W., and Hallett, J.: Microphysical characterization of mixed-phase clouds, *Q. J. Roy. Meteor. Soc.*, 129, 39–65, doi:10.1256/qj.01.204, 2003.
- Korolev, A. V., Emery, E. F., Strapp, J. W., Cober, S. G., Isaac, G. A., Wasey, M., and Marcotte, D.: Small Ice Particles in Tropospheric Clouds: Fact or Artifact? Airborne Icing Instrumentation Evaluation Experiment, *B. Am. Meteorol. Soc.*, 92, 967–973, doi:10.1175/2010BAMS3141.1, 2011.
- Kupiszewski, P., Leck, C., Tjernström, M., Sjogren, S., Sedlar, J., Graus, M., Müller, M., Brooks, B., Swietlicki, E., Norris, S., and Hansel, A.: Vertical profiling of aerosol particles and trace gases over the central Arctic Ocean during summer, *Atmos. Chem. Phys.*, 13, 12405–12431, doi:10.5194/acp-13-12405-2013, 2013.
- Lance, S., Shupe, M. D., Feingold, G., Brock, C. A., Cozic, J., Holloway, J. S., Moore, R. H., Nenes, A., Schwarz, J. P., Spackman, J. R., Froyd, K. D., Murphy, D. M., Brioude, J., Cooper, O. R., Stohl, A., and Burkhardt, J. F.: Cloud condensation nuclei as a modulator of ice processes in Arctic mixed-phase clouds, *Atmos. Chem. Phys.*, 11, 8003–8015, doi:10.5194/acp-11-8003-2011, 2011.
- Latham, T. L., Beyersdorf, A. J., Thornhill, K. L., Winstead, E. L., Cubison, M. J., Hecobian, A., Jimenez, J. L., Weber, R. J., Anderson, B. E., and Nenes, A.: Analysis of CCN activity of Arctic aerosol and Canadian biomass burning during summer 2008, *Atmos. Chem. Phys.*, 13, 2735–2756, doi:10.5194/acp-13-2735-2013, 2013.
- Lawler, M. J., Whitehead, J., O'Dowd, C., Monahan, C., McFiggans, G., and Smith, J. N.: Composition of 15–85 nm particles in marine air, *Atmos. Chem. Phys.*, 14, 11557–11569, doi:10.5194/acp-14-11557-2014, 2014.
- Lawson, R. P., Baker, B. A., Schmitt, C. G., and Jensen, T. L.: An overview of microphysical properties of Arctic clouds observed in May and July 1998 during FIRE ACE, *J. Geophys. Res.-Atmos.*, 106, 14989–15014, doi:10.1029/2000JD900789, 2001.
- Leaith, W. R., Sharma, S., Huang, L., Toom-Saunty, D., Chivulescu, A., Macdonald, A. M., von Salzen, K., Pierce, J. R., Bertram, A. K., Schroder, J. C., Shantz, N. C., Chang, R. Y.-W., and Norman, A.-L.: Dimethyl sulfide control of the clean summertime Arctic aerosol and cloud, *Elem. Sci. Anthr.*, 1, 000017, doi:10.12952/journal.elementa.000017, 2013.
- Lebsock, M. D., Stephens, G. L., and Kummerow, C.: Multisensor satellite observations of aerosol effects on warm clouds, *J. Geophys. Res.-Atmos.*, 113, D15205, doi:10.1029/2008JD009876, 2008.

- Leck, C. and Bigg, E. K.: Aerosol production over remote marine areas-A new route, *Geophys. Res. Lett.*, 26, 3577–3580, doi:10.1029/1999GL010807, 1999.
- Lihavainen, H., Kerminen, V.-M., and Remer, L. A.: Aerosol-cloud interaction determined by both in situ and satellite data over a northern high-latitude site, *Atmos. Chem. Phys.*, 10, 10987–10995, doi:10.5194/acp-10-10987-2010, 2010.
- Lindsey, D. T. and Fromm, M.: Evidence of the cloud lifetime effect from wildfire-induced thunderstorms, *Geophys. Res. Lett.*, 35, L22809, doi:10.1029/2008GL035680, 2008.
- Lohmann, U. and Leck, C.: Importance of submicron surface-active organic aerosols for pristine Arctic clouds, *Tellus B*, 57, 261–268, doi:10.3402/tellusb.v57i3.16534, 2005.
- Lubin, D. and Vogelmann, A. M.: A climatologically significant aerosol longwave indirect effect in the Arctic, *Nature*, 439, 453–456, doi:10.1038/nature04449, 2006.
- Matsui, H., Kondo, Y., Moteki, N., Takegawa, N., Sahu, L. K., Zhao, Y., Fuelberg, H. E., Sessions, W. R., Diskin, G., Blake, D. R., Wisthaler, A., and Koike, M.: Seasonal variation of the transport of black carbon aerosol from the Asian continent to the Arctic during the ARCTAS aircraft campaign, *J. Geophys. Res. Atmos.*, 116, D05202, doi:10.1029/2010JD015067, 2011.
- McComiskey, A. and Feingold, G.: Quantifying error in the radiative forcing of the first aerosol indirect effect, *Geophys. Res. Lett.*, 35, L02810, doi:10.1029/2007GL032667, 2008.
- McComiskey, A. and Feingold, G.: The scale problem in quantifying aerosol indirect effects, *Atmos. Chem. Phys.*, 12, 1031–1049, doi:10.5194/acp-12-1031-2012, 2012.
- McComiskey, A., Feingold, G., Frisch, A. S., Turner, D. D., Miller, M. A., Chiu, J. C., Min, Q., and Ogren, J. A.: An assessment of aerosol-cloud interactions in marine stratus clouds based on surface remote sensing, *J. Geophys. Res.-Atmos.*, 114, D09203, doi:10.1029/2008JD011006, 2009.
- McConnell, J. R., Edwards, R., Kok, G. L., Flanner, M. G., Zender, C. S., Saltzman, E. S., Banta, J. R., Pasteris, D. R., Carter, M. M., and Kahl, J. D. W.: 20th-Century Industrial Black Carbon Emissions Altered Arctic Climate Forcing, *Science*, 317, 1381–1384, doi:10.1126/science.1144856, 2007.
- McFarquhar, G. M., Zhang, G., Poellot, M. R., Kok, G. L., McCoy, R., Tooman, T., Fridlind, A., and Heymsfield, A. J.: Ice properties of single-layer stratocumulus during the Mixed-Phase Arctic Cloud Experiment: 1. Observations, *J. Geophys. Res.-Atmos.*, 112, D24201, doi:10.1029/2007JD008633, 2007.
- McFarquhar, G. M., Ghan, S., Verlinde, J., Korolev, A., Strapp, J. W., Schmid, B., Tomlinson, J. M., Wolde, M., Brooks, S. D., Cziczo, D., Dubey, M. K., Fan, J., Flynn, C., Gultepe, I., Hubbe, J., Gilles, M. K., Laskin, A., Lawson, P., Leaitch, W. R., Liu, P., Liu, X., Lubin, D., Mazzoleni, C., Macdonald, A.-M., Moffet, R. C., Morrison, H., Ovchinnikov, M., Shupe, M. D., Turner, D. D., Xie, S., Zelenyuk, A., Bae, K., Freer, M., and Glen, A.: Indirect and semi-direct aerosol campaign: The Impact of Arctic Aerosols on Clouds, *B. Am. Meteorol. Soc.*, 92, 183–201, 2011.
- Moore, R. H., Bahreini, R., Brock, C. A., Froyd, K. D., Cozic, J., Holloway, J. S., Middlebrook, A. M., Murphy, D. M., and Nenes, A.: Hygroscopicity and composition of Alaskan Arctic CCN during April 2008, *Atmos. Chem. Phys.*, 11, 11807–11825, doi:10.5194/acp-11-11807-2011, 2011.
- Moore, R. H., Karydis, V. A., Capps, S. L., Latham, T. L., and Nenes, A.: Droplet number uncertainties associated with CCN: an assessment using observations and a global model adjoint, *Atmos. Chem. Phys.*, 13, 4235–4251, doi:10.5194/acp-13-4235-2013, 2013.
- Morales, R. and Nenes, A.: Characteristic updrafts for computing distribution-averaged cloud droplet number and stratocumulus cloud properties, *J. Geophys. Res.-Atmos.*, 115, D18220, doi:10.1029/2009JD013233, 2010.
- Morales, R., Nenes, A., Jonsson, H., Flagan, R. C., and Seinfeld, J. H.: Evaluation of an entraining droplet activation parameterization using in situ cloud data, *J. Geophys. Res.-Atmos.*, 116, D15205, doi:10.1029/2010JD015324, 2011.
- Moritz, M. A., Parisien, M.-A., Battlori, E., Krawchuk, M. A., Van Dorn, J., Ganz, D. J., and Hayhoe, K.: Climate change and disruptions to global fire activity, *Ecosphere*, 3, 49, doi:10.1890/ES11-00345.1, 2012.
- Morrison, H., de Boer, G., Feingold, G., Harrington, J., Shupe, M. D., and Sulia, K.: Resilience of persistent Arctic mixed-phase clouds, *Nat. Geosci.*, 5, 11–17, doi:10.1038/ngeo1332, 2012.
- Moteki, N. and Kondo, Y.: Method to measure time-dependent scattering cross sections of particles evaporating in a laser beam, *J. Aerosol. Sci.*, 39, 348–364, doi:10.1016/j.jaerosci.2007.12.002, 2008.
- O'Dowd, C., Monahan, C., and Dall'Osto, M.: On the occurrence of open ocean particle production and growth events, *Geophys. Res. Lett.*, 37, L19805, doi:10.1029/2010GL044679, 2010.
- Orellana, M. V., Matrai, P. A., Leck, C., Rauschenberg, C. D., Lee, A. M., and Coz, E.: Marine microgels as a source of cloud condensation nuclei in the high Arctic, *Proc. Natl. Acad. Sci.*, 108, 13612–13617, doi:10.1073/pnas.1102457108, 2011.
- Peng, Y., Lohmann, U., Leaitch, R., Banic, C., and Couture, M.: The cloud albedo-cloud droplet effective radius relationship for clean and polluted clouds from RACE and FIRE.ACE, *J. Geophys. Res.-Atmos.*, 107, AAC 1–1, doi:10.1029/2000JD000281, 2002.
- Platnick, S., King, M. D., Ackerman, S. A., Menzel, W. P., Baum, B. A., Riedi, J. C., and Frey, R. A.: The MODIS cloud products: algorithms and examples from Terra, *IEEE Trans. Geosci. Remote Sens.*, 41, 459–473, doi:10.1109/TGRS.2002.808301, 2003.
- Quinn, P. K., Bates, T. S., Miller, T. L., Coffman, D. J., Johnson, J. E., Harris, J. M., Ogren, J. A., Forbes, G., Anderson, T. L., Covert, D. S., and Rood, M. J.: Surface submicron aerosol chemical composition: What fraction is not sulfate?, *J. Geophys. Res.-Atmos.*, 105, 6785–6805, doi:10.1029/1999JD901034, 2000.
- Quinn, P. K., Miller, T. L., Bates, T. S., Ogren, J. A., Andrews, E., and Shaw, G. E.: A 3-year record of simultaneously measured aerosol chemical and optical properties at Barrow, Alaska, *J. Geophys. Res.*, 107, 4130, doi:10.1029/2001JD001248, 2002.
- Raatikainen, T., Moore, R. H., Latham, T. L., and Nenes, A.: A coupled observation – modeling approach for studying activation kinetics from measurements of CCN activity, *Atmos. Chem. Phys.*, 12, 4227–4243, doi:10.5194/acp-12-4227-2012, 2012.
- Rangno, A. L. and Hobbs, P. V.: Ice particles in stratiform clouds in the Arctic and possible mechanisms for the production of high ice concentrations, *J. Geophys. Res.-Atmos.*, 106, 15065–15075, doi:10.1029/2000JD900286, 2001.
- R Core Team: R: A language and environment for statistical computing. R Foundation for Statistical Computing, Vienna, Austria, available at: <http://www.R-project.org/> (last access: 1 November 2015), 2013.

- Rosenfeld, D., Fromm, M., Trentmann, J., Luderer, G., Andreae, M. O., and Servranckx, R.: The Chisholm firestorm: observed microstructure, precipitation and lightning activity of a pyro-cumulonimbus, *Atmos. Chem. Phys.*, 7, 645–659, doi:10.5194/acp-7-645-2007, 2007.
- Rosenfeld, D., Wang, H., and Rasch, P. J.: The roles of cloud drop effective radius and LWP in determining rain properties in marine stratocumulus, *Geophys. Res. Lett.*, 39, L13801, doi:10.1029/2012GL052028, 2012.
- Rosenfeld, D., Fischman, B., Zheng, Y., Goren, T., and Giguzin, D.: Combined satellite and radar retrievals of drop concentration and CCN at convective cloud base, *Geophys. Res. Lett.*, 41, 2014GL059453, doi:10.1002/2014GL059453, 2014.
- Sachse, G. W., Hill, G. F., Wade, L. O., and Perry, M. G.: Fast response, high precision carbon monoxide sensor using a tunable diode laser absorption technique, *J. Geophys. Res.*, 92, 2071–2081, 1987.
- Sakamoto, K. M., Allan, J. D., Coe, H., Taylor, J. W., Duck, T. J., and Pierce, J. R.: Aged boreal biomass-burning aerosol size distributions from BORTAS 2011, *Atmos. Chem. Phys.*, 15, 1633–1646, doi:10.5194/acp-15-1633-2015, 2015.
- Seinfeld, J. H. and Pandis, S. N.: *Atmospheric Chemistry and Physics: From Air Pollution to Climate Change*, John Wiley and Sons, New York, 1998.
- Sen, P. K.: Estimates of the Regression Coefficient Based on Kendall's Tau, *J. Am. Stat. Assoc.*, 63, 1379–1389, doi:10.1080/01621459.1968.10480934, 1968.
- Shantz, N. C., Gultepe, I., Liu, P. S. K., Earle, M. E., and Zelenyuk, A.: Spatial and temporal variability of aerosol particles in Arctic spring, *Q. J. Roy. Meteor. Soc.*, 138, 2229–2240, doi:10.1002/qj.1940, 2012.
- Shantz, N. C., Gultepe, I., Andrews, E., Zelenyuk, A., Earle, M. E., Macdonald, A. M., Liu, P. S. K., and Leaitch, W. R.: Optical, physical, and chemical properties of springtime aerosol over Barrow Alaska in 2008, *Int. J. Climatol.*, 34, 3125–3138, doi:10.1002/joc.3898, 2014.
- Shao, H. and Liu, G.: Influence of mixing on evaluation of the aerosol first indirect effect, *Geophys. Res. Lett.*, 33, L14809, doi:10.1029/2006GL026021, 2006.
- Shaw, G. E.: The Arctic Haze Phenomenon, *B. Am. Meteorol. Soc.*, 76, 2403–2413, doi:10.1175/1520-0477(1995)076<2403:TAHP>2.0.CO;2, 1995.
- Soja, A. J., Stocks, B., Maczek, P., Fromm, M., Servranckx, R., and Turetsky, M.: ARCTAS: the perfect smoke, *Can. Smoke Newsl.*, 2–7, 2008.
- Stephens, G. L.: Radiation Profiles in Extended Water Clouds, I: Theory, *J. Atmospheric Sci.*, 35, 2111–2122, doi:10.1175/1520-0469(1978)035<2111:RPIEWC>2.0.CO;2, 1978.
- Stocks, B. J., Fosberg, M. A., Lynham, T. J., Mearns, L., Wotton, B. M., Yang, Q., Jin, J.-Z., Lawrence, K., Hartley, G. R., Mason, J. A., and McKenney, D. W.: Climate Change and Forest Fire Potential in Russian and Canadian Boreal Forests, *Climatic Change*, 38, 1–13, doi:10.1023/A:1005306001055, 1998.
- Stohl, A., Andrews, E., Burkhart, J. F., Forster, C., Herber, A., Hoch, S. W., Kowal, D., Lunder, C., Mefford, T., Ogren, J. A., Sharma, S., Spichtinger, N., Stebel, K., Stone, R., Ström, J., Tørseth, K., Wehrli, C., and Yttri, K. E.: Pan-Arctic enhancements of light absorbing aerosol concentrations due to North American boreal forest fires during summer 2004, *J. Geophys. Res.*, 111, D22214, doi:10.1029/2006JD007216, 2006.
- Stohl, A., Berg, T., Burkhart, J. F., Fjårraa, A. M., Forster, C., Herber, A., Hov, Ø., Lunder, C., McMillan, W. W., Oltmans, S., Shiobara, M., Simpson, D., Solberg, S., Stebel, K., Ström, J., Tørseth, K., Treffeisen, R., Virkkunen, K., and Yttri, K. E.: Arctic smoke – record high air pollution levels in the European Arctic due to agricultural fires in Eastern Europe in spring 2006, *Atmos. Chem. Phys.*, 7, 511–534, doi:10.5194/acp-7-511-2007, 2007.
- Stone, R. S.: Variations in western Arctic temperatures in response to cloud radiative and synoptic-scale influences, *J. Geophys. Res.-Atmos.*, 102, 21769–21776, doi:10.1029/97JD01840, 1997.
- Strapp, J. W., Leaitch, W. R., and Liu, P. S. K.: Hydrated and Dried Aerosol-Size-Distribution Measurements from the Particle Measuring Systems FSSP-300 Probe and the Deiced PCASP-100X Probe, *J. Atmos. Ocean. Technol.*, 9, 548–555, doi:10.1175/1520-0426(1992)009<0548:HADASD>2.0.CO;2, 1992.
- Ström, J., Engvall, A.-C., Delbart, F., Krejci, R. and Treffeisen, R.: On small particles in the Arctic summer boundary layer: observations at two different heights near Ny-Ålesund, Svalbard, *Tellus B*, 61, 473–482, doi:10.3402/tellusb.v61i2.16845, 2009.
- Tao, W.-K., Chen, J.-P., Li, Z., Wang, C., and Zhang, C.: Impact of aerosols on convective clouds and precipitation, *Rev. Geophys.*, 50, RG2001, doi:10.1029/2011RG000369, 2012.
- Theil, H.: A rank-invariant method of linear and polynomial regression analysis, *Proc. R. Neth. Acad. Sci. LIII*, 1397–1412, 1950.
- Tietze, K., Riedi, J., Stohl, A., and Garrett, T. J.: Space-based evaluation of interactions between aerosols and low-level Arctic clouds during the Spring and Summer of 2008, *Atmos. Chem. Phys.*, 11, 3359–3373, doi:10.5194/acp-11-3359-2011, 2011.
- Tunved, P., Ström, J., and Krejci, R.: Arctic aerosol life cycle: linking aerosol size distributions observed between 2000 and 2010 with air mass transport and precipitation at Zeppelin station, Ny-Ålesund, Svalbard, *Atmos. Chem. Phys.*, 13, 3643–3660, doi:10.5194/acp-13-3643-2013, 2013.
- Twomey, S.: The Influence of Pollution on the Shortwave Albedo of Clouds, *J. Atmospheric Sci.*, 34, 1149–1152, doi:10.1175/1520-0469(1977)034<1149:TlOPOT>2.0.CO;2, 1977.
- Vavrus, S., Holland, M. M., and Bailey, D. A.: Changes in Arctic clouds during intervals of rapid sea ice loss, *Clim. Dynam.*, 36, 1475–1489, doi:10.1007/s00382-010-0816-0, 2010.
- Warneke, C., Bahreini, R., Brioude, J., Brock, C. A., Gouw, J. A. de, Fahey, D. W., Froyd, K. D., Holloway, J. S., Middlebrook, A., Miller, L., Montzka, S., Murphy, D. M., Peischl, J., Ryerson, T. B., Schwarz, J. P., Spackman, J. R., and Veres, P.: Biomass burning in Siberia and Kazakhstan as an important source for haze over the Alaskan Arctic in April 2008, *Geophys. Res. Lett.*, 36, L02813, doi:10.1029/2008GL036194, 2009.
- Warneke, C., Froyd, K. D., Brioude, J., Bahreini, R., Brock, C. A., Cozic, J., de Gouw, J. A., Fahey, D. W., Ferrare, R., Holloway, J. S., Middlebrook, A. M., Miller, L., Montzka, S., Schwarz, J. P., Sodemann, H., Spackman, J. R., and Stohl, A.: An important contribution to springtime Arctic aerosol from biomass burning in Russia, *Geophys. Res. Lett.*, 37, L01801, doi:10.1029/2009gl041816, 2010.
- Wisthaler, A., Hansel, A., Dickerson, R. R., and Crutzen, P. J.: Organic trace gas measurements by PTR-MS dur-

- ing INDOEX 1999, *J. Geophys. Res.-Atmos.*, 107, 8024, doi:10.1029/2001JD000576, 2002.
- Zelenyuk, A., Yang, J., Choi, E., and Imre, D.: SPLAT II: An Aircraft Compatible, Ultra-Sensitive, High Precision Instrument for In-Situ Characterization of the Size and Composition of Fine and Ultrafine Particles, *Aerosol Sci. Technol.*, 43, 411–424, doi:10.1080/02786820802709243, 2009.
- Zelenyuk, A., Imre, D., Earle, M., Easter, R., Korolev, A., Leaitch, R., Liu, P., Macdonald, A. M., Ovchinnikov, M., and Strapp, W.: In Situ Characterization of Cloud Condensation Nuclei, Interstitial, and Background Particles Using the Single Particle Mass Spectrometer, SPLAT II, *Anal. Chem.*, 82, 7943–7951, doi:10.1021/ac1013892, 2010.
- Zelenyuk, A., Imre, D., Wilson, J., Zhang, Z., Wang, J., and Mueller, K.: Airborne single particle mass spectrometers (SPLAT II & miniSPLAT) and new software for data visualization and analysis in a geo-spatial context, *J. Am. Soc. Mass Spectrom.*, 26, 257–270, doi:10.1007/s13361-014-1043-4, 2015.
- Zhao, C. and Garrett, T. J.: Effects of Arctic haze on surface cloud radiative forcing, *Geophys. Res. Lett.*, 42, 2014GL062015, doi:10.1002/2014GL062015, 2015.
- Zhao, C., Klein, S. A., Xie, S., Liu, X., Boyle, J. S., and Zhang, Y.: Aerosol first indirect effects on non-precipitating low-level liquid cloud properties as simulated by CAM5 at ARM sites, *Geophys. Res. Lett.*, 39, L08806, doi:10.1029/2012GL051213, 2012.
- Zhou, J., Swietlicki, E., Berg, O. H., Aalto, P. P., Hämeri, K., Nilsson, E. D., and Leck, C.: Hygroscopic properties of aerosol particles over the central Arctic Ocean during summer, *J. Geophys. Res.-Atmos.*, 106, 32111–32123, doi:10.1029/2000JD900426, 2001.
- Zuidema, P., Baker, B., Han, Y., Intrieri, J., Key, J., Lawson, P., Matrosov, S., Shupe, M., Stone, R., and Uttal, T.: An Arctic Springtime Mixed-Phase Cloudy Boundary Layer Observed during SHEBA, *J. Atmos. Sci.*, 62, 160–176, doi:10.1175/JAS-3368.1, 2005.